Merle, R., Amelin, Y., Yin, Q.-Z., Huyskens, M. H., Sanborn, M. E., Nagashima, K., Yamashita, K., Ireland, T. R., Krot, A. N., Sieber, M. (2020): Exploring the efficiency of stepwise dissolution in removal of stubborn non-radiogenic Pb in chondrule U-Pb dating. - Geochimica et Cosmochimica Acta, 277, 1-20.

https://doi.org/10.1016/j.gca.2020.03.010

EXPLORING THE EFFICIENCY OF STEPWISE DISSOLUTION IN REMOVAL OF STUBBORN NON-RADIOGENIC PB IN CHONDRULE U-PB DATING

Renaud Merle[1*], Yuri Amelin[1], Qing-Zhu Yin[2], Magdalena H. Huyskens[2], Matthew E. Sanborn[2], Kazuhide Nagashima[3], Katsuyuki Yamashita[4], Trevor R. Ireland[1], Alexander N. Krot[3], Melanie J. Sieber[1,5]

[1]*Research School of Earth Sciences, The Australian National University, Canberra, 2601 Australia*

[2]*Department of Earth and Planetary Sciences, University of California-Davis, One Shields Avenue, Davis, CA, USA*

[3]*Hawai'i Institute of Geophysics and Planetology, University of Hawai'i at Mānoa, Honolulu, HI 96822, USA*

[4]*Graduate School of Natural Science and Technology, Okayama University, Japan*

[5]*GFZ, German Research Centre for Geoscience, Telegrafenberg, D.-14473 Potsdam, Germany*

*Corresponding author: Renaud Merle

Present address: Swedish Museum of Natural History,
Box 50007
104 05 Stockholm

Abstract

Chondrules in chondritic meteorites are unique witnesses of nebular and asteroidal processes that preceded large-scale planetary accretion. Together with refractory calcium-aluminium-rich inclusions (CAIs), they are the sources of our knowledge of the initial evolution of the early Solar System. We have investigated a single very large (>10 mm in longer dimension) chondrule, hereafter, the mega-chondrule A25-2, extracted from the Allende CV3 chondrite. We characterised texture, mineralogy and mineral chemistry of this chondrule, and studied its Al-Mg, U-Pb and U-isotope systematics. We also studied the distribution of U, Th and Pb, and measured Pb isotopic composition in individual minerals of A25-2 by secondary ion mass-spectrometry (SIMS). The main difficulty in absolute age determination was the presence of pervasive and resilient non-radiogenic Pb. In the search for the best way to separate radiogenic Pb from non-radiogenic Pb components of terrestrial and asteroidal origins, we used various protocols of multi-step leaching and assessed their efficiency in generating data suitable for the construction of an isochron. Testing the data filtering procedure led us to explore the behaviour of the stepwise leaching method in the presence of pervasive and resilient non-radiogenic Pb. The model age patterns observed in the final HF partial dissolution steps probably induced isotopic fractionation. Although step leaching did not yield fractions with highly radiogenic Pb, a Pb-Pb isochron age corrected for measured $^{238}U/^{235}U$ was obtained by: (1) data filtering process based on strict analytical and geochemical criteria to include in the Pb-Pb isochron only leaching steps free from terrestrial contamination and (2) arithmetically recombined analyses to cancel the effects of leaching-induced isotopic fractionation.

This extensive data processing yielded the age of 4568.5±3.0 Ma, which we consider reliable within its uncertainty limits, although it is not as precise as, and more model dependent than, the age that could have been obtained if Pb isotopic compositions were more

radiogenic. The $^{238}U/^{235}U$ ratio of the mega-chondrule is 137.764±0.016, which is similar to the ratios obtained from single chondrules yet slightly different from small pooled Allende chondrules. The initial $^{27}Al/^{26}Al$ ratio inferred from internal isochron obtained from SIMS Al-Mg isotope measurements is $(5.4\pm6.5)\times10^{-6}$, which corresponds to 4565.0 +0.8/-∞ Ma, assuming homogeneous distribution of ^{26}Al throughout the protoplanetary disk at the canonical level ($\sim5.2\times10^{-5}$). This age is 3.5±3.1 Ma younger than the Pb-isotopic age. Calculation of ^{26}Al-^{26}Mg age assuming initial $(^{27}Al/^{26}Al)_0$ of $(1.36\pm0.72)\times10^{-5}$ in the chondrule-forming region yields the age of 4566.4+0.8/-∞, which is consistent with the Pb-isotopic age.

66 **1. INTRODUCTION**

67 Chondrules, mm-sized spherules of mafic silicate rocks, are one of the major
68 components of chondritic meteorites, and among the oldest solids formed in our Solar
69 System. Chondrules formed in the protoplanetary disk of dust and gas surrounding the proto-
70 Sun (e.g., Desch and Connolly, 2002; Itoh and Yurimoto, 2003; Connelly et al., 2012; Budde
71 et al., 2016; Bollard et al., 2017).

72 Mineralogical, textural, and isotopic observations (e.g., presence of fragments of
73 chondrules of earlier generations as relict grains inside chondrules, U-Pb absolute and Al-Mg
74 relative ages) provide evidence that multiple generations of chondrules, possibly formed in a
75 variety of processes, can be found in an individual chondrite (Connelly et al., 2012; Bollard et
76 al., 2017; Schrader et al., 2017; Krot et al., 2018; Nagashima et al., 2018, Bollard et al. 2019).
77 The "nebular" models of chondrule formation include the currently popular models that
78 consider melting of the nebular condensates by various localised heating processes, e.g., the
79 jet flow (x-wind) model (e.g. Shu et al., 2001) in which the CAIs and chondrules formed near
80 the protosun contemporaneously, and the shock-wave model (Desch et al. 2005) in which
81 CAIs and chondrules are formed in the inner disk (1 to 4 astronomic units from the protosun)
82 as a results of multiple transient heating events generated by shock waves. The
83 "planetesimal" models explain formation of chondrules as droplets of melt derived from
84 already accreted kilometre-sized or larger bodies (planetesimals) through high-energy
85 processes such as collisions. The earlier "planetesimal" models that involve low-velocity
86 collisions between partially molten planetesimals (Asphaug et al., 2011; Sanders and Scott,
87 2012) cannot explain primitive chemical compositions of chondrules (Bland et al., 2005) and
88 magnetic properties of chondrites (Weiss and Elkins-Tanton 2013). A more recent model of
89 high-energy collisions between the solid bodies with variable porosity (Johnson et al. 2014,
90 2015) circumvents these problems and makes the collisional models a viable alternative to

91 the nebular models. Regardless of their formation mechanism, the age of chondrules has been
92 used to constrain the lifetime of the protoplanetary disk, the timing of giant planet migration,
93 accretion times for planetesimals, the onset of planetary differentiation and thermal
94 processing in the disk. Since the diversity of chondrule populations in individual meteorites
95 has been documented, accurate chondrule age determinations by any isotopic method must
96 rely on analyses of individual chondrules.

97 U-Pb geochronology using isotopic dilution thermal ionisation mass spectrometry
98 (ID-TIMS) is the only long-lived radioisotope chronometer that can provide sufficient time
99 resolution to determine the timing of separate chondrule-forming events. In several cases,
100 high precision Pb-Pb isochron dates for individual chondrules, or small groups of chondrules,
101 have been obtained with a multi-step acid leaching procedure in which radiogenic and non-
102 radiogenic Pb components can be progressively extracted from different mineral phases
103 (Amelin and Krot, 2007; Connelly and Bizzarro, 2009; Connelly et al., 2012; Bollard et al.,
104 2017).

105 The primary goal of this study was to determine the age of an unusually large (> 10 mm,
106 see figure A0 in supplementary material) chondrule A25-2 from the Allende CV3 (Vigarano
107 type) carbonaceous chondrite. This age determination is supported by measurement of the
108 $^{238}U/^{235}U$ isotopic ratio in this mega-chondrule. We also determined the Pb isotopic
109 composition of the Allende matrix as a possible proxy for any initial Pb component that could
110 have been present in the mega-chondrule along with primordial Pb. Furthermore, we
111 attempted to investigate the short-lived ^{26}Al-^{26}Mg system (^{26}Al decays to ^{26}Mg with a half-
112 life of 0.705 Myr; e.g., Norris et al., 1983).

113 The mega-chondrule A25-2 contains significant amount of both initial and terrestrial Pb
114 compared to the amount of radiogenic Pb. In an effort to separate radiogenic and non-
115 radiogenic Pb components for the purpose of constructing a meaningful Pb-Pb isochron, we

investigated the effects of the step dissolution procedure on the U-Pb system. As the mega-chondrule A25-2 failed to yield a precise Pb-Pb isochron age, we show the limits of the step-leaching method in single chondrule geochronology and provide suggestions for an optimal chemical protocol for a given chondrule or meteorite. We achieved this by combining U-Pb isotopic data with mineralogical information, electron microprobe data, and Th-U-Pb abundances measured by secondary ion mass spectrometry (SIMS) in mesostasis and mineral phases.

2. PREVIOUS U-PB AND AL-MG ISOTOPIC STUDIES OF ALLENDE CHONDRULES

The Allende meteorite is an oxidized CV3 carbonaceous chondrite that experienced iron-alkali metasomatic alteration and relatively mild thermal metamorphism with peak temperature of ~500°C (e.g., Guimon et al., 1995; Krot et al., 1998; Bonal et al., 2006; Cody et al., 2008). The average size of chondrules in the CV chondites is about 1 mm (e.g., Weisberg et al., 2006), but some chondrules are significantly larger (e.g., Tanaka et al., 1975).

Allende has been extensively investigated since its fall and recovery in 1969, yet the available isotopic and chronological data concerning its chondrules are not abundant. These data are briefly described in the following section. All the uncertainties are given at 2σ level.

2.1. $^{238}U/^{235}U$ ratios

The $^{238}U/^{235}U$ ratio must be accurately known for calculation of U-Pb and Pb-Pb dates. Until 2010, the $^{238}U/^{235}U$ isotopic ratio in the early Solar System materials was assumed to be

139 constant and equal to 137.88. Brennecka et al. (2010) first demonstrated substantial variations
140 of this ratio in CV CAIs that indicated the need for corrections to the calculated $^{207}Pb/^{206}Pb$
141 ages. Five $^{238}U/^{235}U$ determinations are available for the Allende chondrules: two sets of
142 pooled chondrules yielded $^{238}U/^{235}U$ ratios of 137.724±0.040 (Amelin et al., 2010) and
143 137.786±0.004 (Brennecka et al., 2015), respectively. These values are distinct, but both
144 overlap within uncertainties with those measured in bulk Allende chondrite that range from
145 137.747±0.017 to 137.817±0.033 (Stirling et al., 2005, 2006; Amelin et al., 2010; Brennecka
146 et al., 2010; Goldmann et al., 2015). Three individual chondrules yielded ratios ranging from
147 137.772±0.014 to 137.779±0.016 (recalculated from Connelly et al., 2012, using a CRM
148 112a standard value of 137.837 according to Richter et al., 2010) to make it comparable to
149 the reported bulk rock values).

150

151 **2.2. Pb-Pb dates of Allende chondrules**

152 Modern U-Pb ID-TIMS techniques have sufficient sensitivity to date relatively large
153 single chondrules. So far, there are seven Pb-Pb ages on Allende chondrules, among which
154 five have precision better than 1 Ma. In the following section, the published Pb-Pb age of
155 Allende chondrules are given as published (i.e. calculated with $^{238}U/^{235}U$=137.88 of Steiger
156 and Jäger (1977) for pre-2010 studies. For more recent studies, we use either directly
157 measured $^{238}U/^{235}U$ (if such data are available), or $^{238}U/^{235}U$=137.786 of Connelly et al.
158 (2012).

159 The first two Pb-Pb isochron ages calculated from a mixture of various components
160 (chondrules, matrix, and CAIs) yielded 4553±4 Ma and 4565±4 Ma (Chen and Tilton, 1976;
161 Tatsumoto et al., 1976). More recently, eight internal isochrons based on step-leaching multi-
162 chondrule fractions produced consistent ages and yielded a weighted average age of

163 4566.6±1.0 Ma (Amelin and Krot, 2007). This data set has been combined with data obtained
164 by step-leaching from a single set of multiple chondrules and the resulting dataset yielded an
165 isochron age of 4565.45±0.45 Ma (Connelly et al., 2008). A similar isochron age of
166 4565.32±0.81 Ma has been obtained from a set of ten chondrules processed by a ten-steps
167 leaching protocol (Connelly and Bizzarro, 2009). More recently, two step-leaching isochrons
168 on single chondrules yielded the ages of 4567.32±0.42 Ma and 4566.24±0.63 Ma (Connelly
169 et al., 2012). Note that none of these ages were calculated using a $^{238}U/^{235}U$ ratio measured in
170 the same chondrule.
171

172 **2.3. ^{26}Al-^{26}Mg system**

173 Short-lived extinct radionuclide ^{26}Al is thought to have been produced in one or several
174 nearby stars of the proto Solar System and injected into the protosolar molecular cloud
175 shortly before or during its collapse (e.g., Krot et al., 2012 and references therein). The decay
176 of this radionuclide to ^{26}Mg is used for high resolution dating of the Solar System processes,
177 assuming that ^{26}Al was homogeneously distributed in the solar nebula (e.g., Lee et al., 1976;
178 Dauphas and Chaussidon, 2011; Kita and Ushikubo, 2012; Kita et al., 2013). Crystallization
179 ages of chondrules relative to the formation of the Solar System can be calculated if the initial
180 $^{26}Al/^{27}Al$ ratio [$(^{26}Al/^{27}Al)_0$] in the Solar System is known. The $(^{26}Al/^{27}Al)_0$ of $\sim 5.2\times10^{-5}$
181 derived from high-precision Al-Mg isotope measurements of CV CAIs by MC-ICP-MS
182 (Jacobsen et al., 2008; MacPherson et al., 2010, 2012, Kawasaki et al., 2019) is commonly
183 considered to represent the initial $^{26}Al/^{27}Al$ ratio in the Solar System and called the canonical
184 ratio. Assuming uniform distribution of ^{26}Al in the solar nebula at the canonical level, the
185 internal Al-Mg isochrons of chondrules from unmetamorphosed (type 2–3.0) chondrites
186 measured by SIMS suggest formation of chondrules between 1 to 4 Ma after the canonical

187 CAIs (Villeneuve et al., 2009; Kita and Ushikubo, 2012; Kita et al., 2013; Luu et al., 2015;
188 Schrader et al., 2017; Nagashima et al., 2019; Pape et al., 2019).

189 So far, ~30 Allende chondrules have been investigated by MC-SIMS or MC-ICP-MS for
190 internal (mineral) isochrons determination. The calculated $(^{26}Al/^{27}Al)_0$ ratios range from
191 $(2.80\pm1.30)\times10^{-6}$ to $(2.59\pm1.53)\times10^{-5}$ (Hutcheon et al., 2009; Luu et al., 2015). The bulk
192 Allende chondrule model isochrons yielded initial ratios ranging from $(5.66\pm0.80)\times10^{-5}$ to
193 $(1.23\pm0.21)\times10^{-5}$ (Bizzarro et al., 2004; Luu et al., 2015). Note that the range of the initial
194 ratios obtained from internal isochrons overlaps the range of the initial $^{26}Al/^{27}Al$ ratios from
195 bulk isochrons.

196 Assuming homogeneous distribution of ^{26}Al in the Solar System at the canonical level,
197 the initial $^{26}Al/^{27}Al$ ratios calculated from mineral isochrons suggest that chondrule formation
198 was either a process initiated during CAI formation and lasted for 2–3 Ma (Bizzarro et al.,
199 2004) or occurred ~ 1.2 Ma to ~4 Ma after condensation of the first solids (Villeneuve et al.,
200 2009; Luu et al., 2015). The variation of the initial $^{26}Al/^{27}Al$ ratio observed among chondrules
201 from a given meteorite implies age differences of 0.5 to 2 Ma (e.g., Kurahashi et al., 2008;
202 Pape et al., 2019). The statistical tests in Schrader et al. (2016) suggest multiple generations
203 of chondrules in each chondrite group. These observations reinforce the requirement of using
204 single chondrules, rather than multi-chondrule fractions, for age determination.
205

206 **3. METHODS**

207 The Allende mega-chondrule A25-2 was selected for this study as it was large enough to
208 be split into multiple fractions (Fig. A0 in Supplementary Material) and could be investigated
209 using different methods. The full description of the sample, the methodological approach and
210 the analytical protocols are given in supplementary material (EA 1-text file).

211 The texture and mineral chemistry of the mega-chondrule A25-2 were investigated by
212 energy dispersive x-ray spectroscopy and electron microprobe analysis at The Australian
213 National University (ANU) and the University of Hawai‘i (full details in EA 1-text file and
214 complete dataset in EA-dataset 1, Fig. A1 in Supplementary Material). The uranium isotopic
215 ratios were measured by Multi-Collection Inductively Coupled Plasma Mass Spectrometry
216 (MC-ICP-MS) at the University of California-Davis (EA-dataset 2, Fig. A2 in Supplementary
217 Material). The *in-situ* Al-Mg measurements were made in the different phases by SIMS at the
218 University of Hawai‘i (see analytical details in EA 1-text file). The U-Pb systematics
219 determined in the mega-chondrule A25-2 and the Allende matrix were performed by Thermal
220 Ionisation Mass Spectrometry (TIMS: Pb isotopic ratios and concentrations) and MC-ICP-
221 MS (U concentrations) at The Australian National University (EA-dataset 3 and EA-dataset
222 4; Figs. A3a and b, Figs. A4a and b). The mineral U, Pb and Th concentrations were analysed
223 *in situ* by Sensitive High Resolution Ion Probe (SHRIMP) at The Australian National
224 University (see analytical methods in EA-text file, Fig. A5).
225

226 **4. RESULTS**

227 **4.1. Mineralogy and petrology**

228 The mega-chondrule A25-2 has a barred olivine (BO) texture with a framework of
229 elongated up to 100 μm-long olivine crystals (~74 vol%) and xenomorphic high-Ca
230 pyroxenes (~12 vol%) that crystallised between the olivines and scattered Cr-spinels (~0.2
231 vol%; Fig. 1). The remaining volume (~14%) is occupied by mesostasis composed of
232 feldspathic glass and fine-grained high-Ca pyroxene microcrysts (Fig. 1).

233 The representative compositions of these minerals are given in Table 1. The full set of
234 EMPA analyses is given in Table A1 in the Supplementary Material (EA-dataset 1).

235 The olivines have ferroan composition ($Fa_{26–30}$) and, thus, the chondrule is
236 categorized as type II BO chondrule (Jones et al., 2005). The pyroxenes show a large variety
237 of composition ranging from low-Ca to high-Ca clinopyroxene ($Fs_{30–48,}$ $Wo_{6–28}$; Al_2O_3 = 3−8
238 wt.%, Table A1 in EA1 dataset). The spinels have a Fe-rich chromite composition (FeO ~ 24
239 wt.%; Cr_2O_3 ~ 40−43 wt%, Table A1 in Supplementary Material).
240 The EDS mapping shows that Na and Al are located in the mesostasis in the same
241 areas (Fig. A1 in Supplementary Material). This suggests that the feldspathic glass is rather
242 sodic (Fig. A1 in Supplementary Material). No phosphates or sulphides were unambiguously
243 identified. The potassium content was below detection limit. High calcium contents are
244 located where pyroxene has been identified in the BSE images (Fig. 1 and Fig. A1 in
245 Supplementary Material) suggesting the presence of clinopyroxene.
246
247 **4.2. $^{238}U/^{235}U$ isotopic ratios**
248 The mega-chondrule A25-2 was analysed during two analytical sessions and the results
249 yielded a weighted average $^{238}U/^{235}U$ ratio of 137.764±0.016 and an average U concentration
250 of 12 ppb (Table A2 in EA- dataset 2 and Fig. A2 in supplementary material).
251 This $^{238}U/^{235}U$ ratio overlaps within uncertainty the values obtained from the other
252 individual Allende chondrules (Fig. 2; Connelly et al., 2012) and the multi-chondrule fraction
253 of Amelin et al. (2010). Considering uncertainties of the previously published $^{238}U/^{235}U$, our
254 new ratio for the mega-chondrule A25-2 is also in agreement with both the values obtained
255 for bulk Allende meteorite and the most recent estimate of the Solar System ratio
256 (137.794±0.027, 95% confidence; Goldmann et al., 2015, see Fig. 2). However, our new
257 $^{238}U/^{235}U$ ratio differs from the value of 137.786±0.004 from the Allende multi-chondrule
258 fractions obtained by Brennecka et al. (2015). Note that this latter value overlaps those of the
259 individual chondrules from Connelly et al. (2012), 137.772±0.014 to 137.779±0.016.

260

261 **4.3. Al-Mg systematics**

262 Olivine, clinopyroxene and Cr-spinel were analysed by SIMS for ^{26}Al-^{26}Mg systematics
263 in the mega chondrule. The pervasive presence of fine-grained clinopyroxene in the
264 mesostasis precludes any reliable SIMS analysis from the mega-chondrule A25-2 mesostasis
265 as instrumental mass fractionation and relative sensitivity factor are different depending on
266 the phases analysed. The ^{27}Al/^{24}Mg values ranges from 0.213±0.007 to 0.415±0.014 for
267 clinopyroxene, from 0.00126±0.00004 to 0.00143±0.00005 for olivine, and from 2.2±0.22 to
268 3.3±0.33 for Cr-spinel (Table 2). The analysed minerals do not show resolved excess of
269 radiogenic ^{26}Mg (Table 2). The Cr-spinel, clinopyroxenes, and olivines define an internal
270 isochron yielding an initial ratio $(^{27}Al/^{26}Al)_0$ of $(5.4\pm6.5)\times10^{-6}$ (Fig. 3). This ratio, and its
271 upper limit, are significantly lower than the "canonical" value found in CAIs ($\sim5.2\times10^{-5}$).
272 This ratio is in the range of those inferred from the internal isochrons in Kaba (CV_{oxB}3.1)
273 chondrules that is $(2.9\pm1.7)\times10^{-6}$ to $(6.3\pm1.7)\times10^{-6}$ (Nagashima et al., 2017), but lower than
274 those inferred from the model isochrons of the Allende bulk chondrules (1.23×10^{-5} to
275 5.66×10^{-5}; Bizzarro et al., 2004; Luu et al., 2015). Nevertheless, our new $(^{27}Al/^{26}Al)_0$ ratio is
276 within the range as one other internal isochron of a chondrule from Allende of $(4.0\pm2.7)\text{x}10^{-6}$
277 (Bollard et al., 2019).

278

279 **4.4. Th-U-Pb data from the mega-chondrule A25-2**

280 We applied three different step-leaching protocols to nine whole-rock fractions of the
281 mega-chondrule A25-2 ranging between 2 and 12 mg, in three analytical batches involving 4
282 to 13 steps (see EA-text file in supplementary material). The first batch (A31) consisted of

four grain-size fractions (fraction 1: coarse, fraction 2: medium, and fractions 3 and 4: fine). The second batch (A66) consisted of three small fractions of 2–4 mg that were crushed to produce three different grain sizes (#108: coarse fraction, #111: mid-size fraction and #121: fine fraction; see EA-text file and Fig. A0). In the third batch (A68) we analysed two 10–12 mg fractions (one coarse #3 and one fine #12).

The complete U-Pb dataset of all the mega-chondrule A25-2 fractions, including related blanks and standards, uranium and thorium concentrations measured for each steps of the dissolution procedures as well as the corresponding isotopic ratios are available in the supplementary material (EA- dataset 3). All the uncertainties are given at 2σ level. The data were screened for possible isobaric interferences, mass-independent fractionation and other analytical problems following the procedure outlined in Amelin and Davis (2006) and Amelin et al. (2010), and further described in the supplementary material (see EA-text file, Fig. A6 in Supplementary Material).

4.4.1. Uranium and thorium concentrations

Total U concentrations (sum of concentrations measured in residues and all leachates of a given fraction) range from 13 to 27 ppb (Table A3e in Supplementary Material) and total measured Th concentrations vary from 54 to 103 ppb. These U concentrations are similar to the values previously reported for Allende chondrules (e.g., Amelin and Krot, 2007; Connelly et al., 2008).

Within a given batch, the total U and Th concentrations of the different fractions show relatively small variations. There is generally no correlation between uranium and thorium concentrations and the grain size. For U, concentration increases with increasing grain size in

306 A31, the opposite variation is observed in the two other batches (Table A3e). Such variations
307 are correlated with those of thorium for batch A31 only.
308 The $^{232}Th/^{238}U$ ratio (κ) calculated from the radiogenic $^{208}Pb/^{206}Pb$ isotopic ratios and
309 $^{207}Pb/^{206}Pb$ model dates ranges from 3.9 to 4.2 in the nine different fractions (Table A3e).
310 ***4.4.2. Lead concentrations and isotopic ratios***
311 The total Pb concentrations of the nine analysed fractions vary from 110 to 452 ppb and
312 the quantity of Pb present in each individual leaching step of the nine analysed fractions
313 varies from 3 pg to 949 pg. Batch A68 displays more limited variations of Pb contents (Table
314 A3e). The Pb content variations are not related to the weight of the fraction or to the grain
315 size of the fraction within a given batch. The Pb blank ranges from 0.54 to 1.6 pg and its
316 contribution to the uncertainty of the final calculated ratios becomes minor for analyses with
317 more than 10 pg of Pb. The U blank ranges from 0.10 to 0.19 pg.
318 All Pb isotopic analyses of the mega-chondrule A25-2 fractions yielded relatively
319 unradiogenic $^{206}Pb/^{204}Pb$ ratios. Blank-corrected $^{206}Pb/^{204}Pb$ measured range from 15.6 to
320 61.7 (ratios without blank correction range from 15.36 to 51.75). Except for two data points,
321 the individual steps yielded ratios within a narrow range from 18 to 33. The $^{206}Pb/^{204}Pb$ ratios
322 in the residues are among the lowest and least variable of those documented for Allende
323 chondrules (Krot and Amelin, 2007; Connelly and Bizzarro, 2009; Connelly et al., 2012),
324 making the mega-chondrule A25-2 an object that is exceedingly difficult to precisely and
325 accurately date with the U-Pb method. The data points with the lowest and highest
326 $^{206}Pb/^{204}Pb$ ratios (A68-chond 3 L7a: $^{206}Pb/^{204}Pb = 15.3$ and A66-chond 111 L8: $^{206}Pb/^{204}Pb =$
327 61.7) were measured in the HF leaching steps.
328 The entire dataset occupies a triangular field in the $^{204}Pb/^{206}Pb$ vs. $^{207}Pb/^{206}Pb$ diagram
329 (Fig. 4). The majority of the data show a positive correlation between $^{207}Pb/^{206}Pb$ and
330 $^{204}Pb/^{206}Pb$. Some data trend toward a component with an isotopic composition close to the

331 average modern terrestrial crustal Pb (according to Stacey and Kramers, 1975) used as a
332 proxy of average Pb composition of the Earth's continental crust. The distribution of Pb-
333 isotopic data can be interpreted as a mixing between three Pb components: (1) radiogenic Pb
334 produced by radioactive decay of U in closed system conditions, represented by projection of
335 the data array to the y-axis, (2) a component representing an initial Pb composition with an
336 isotopic composition approximating that of primordial Pb of the Solar System (Tatsumoto et
337 al., 1973, Blichert-Toft et al., 2010), and (3) terrestrial contamination Pb. The data having Pb
338 isotopic ratios trending toward the composition of terrestrial Pb are likely to contain
339 significant amounts of the terrestrial Pb. The latter group includes all data from the first
340 water+acetone wash, the majority of the second step data (HBr step), several third step data
341 (HNO_3 step), one HCl step (A66 chond108-L6) and the two A68 residues. Other fractions
342 may be also contaminated by terrestrial Pb to a lesser degree, but its detection is less
343 straightforward.
344

345 **4.5. U-Pb data from Allende matrix**

346 The complete dataset of the Allende matrix powder and fragment measurements is
347 available in EA4 dataset of the supplementary material. A summary of the results is presented
348 in Table 3 and the data are plotted in Figure 5. The data quality was assessed following the
349 same procedure as for the mega-chondrule A25-2 data. None of the Allende matrix data were
350 rejected because of analytical reasons (see EA4 dataset in Supplementary Material).

351 The Pb concentrations range from 0.93 to 21.5 ppm (Table A4c). The blank-corrected
352 $^{206}Pb/^{204}Pb$ ratios range from 9.550 to 18.649. Powder fractions and fragment fractions
353 display different isotopic ratios and chemical compositions. The three powder fractions have
354 higher $^{206}Pb/^{204}Pb$ ratios (11.593 to 18.649) with $^{206}Pb/^{204}Pb$ ratios increasing with Pb
355 concentration. The fragment fractions display lower blank-corrected $^{206}Pb/^{204}Pb$ ratios

356 ranging from 9.550 to 9.836. These values are among the lowest ratios measured for Allende
357 matrix (Chen and Tilton, 1976; Tatsumoto et al., 1976; Arden and Cassey, 1984). The
358 fraction A117-4 has the lowest ratios measured so far in Allende matrix.
359

360 **4.6. Th-U-Pb distribution in mineral phases**

361 Five olivine crystals, three Cr-spinels and four pyroxene and mesostasis locations were
362 analysed for Th, U, Yb and Pb concentrations, and Pb isotopic compositions, with SHRIMP-
363 RG. Ytterbium has similar compatibility to U and Th during crystallisation of parent mafic
364 melt of the chondrules, but is significantly more abundant, so its distribution helps to verify
365 distribution of U and Th in the minerals where the concentrations of these elements are close
366 to the detection limit.

367 The data are reported in Table 4. In all olivine and pyroxene analyses, the primary beam
368 was placed near the centres of the crystals and the corresponding spots do not overlap the
369 surrounding phases (see Fig. A5 in Supplementary Material). Only one spot meant to be in
370 mesostasis overlaps significantly a neighbouring olivine. Considering placement of the
371 analysis spots away from grain boundaries, and extensive rastering, it is suggested that most
372 of the observed ^{204}Pb corresponds to initial Pb rather than surface contamination. The Cr-
373 spinel grains are very small, therefore the SHRIMP spots overlap slightly neighbouring
374 pyroxenes and possibly mesostasis for one analysis (Cr-sp 4, see Fig. A5 in Supplementary
375 Material).

376 The thorium and uranium contents in olivine, pyroxene and Cr-spinel is below 5 ppb,
377 and in many analyses are below the detection limit of ca. 0.5 ppb. Metosasis contains 19-122
378 ppb U, and appears to the be the main host of U. Olivine and Cr-spinel have lower average
379 ytterbium contents (55 ppb and 88 ppb respectively) than mesostasis (1.4 ppm) and pyroxene
380 (1.5 ppm).

Olivine and mesostasis contain measurable quantities of ^{204}Pb between 1.5 and 11 ppb, while in pyroxene and spinel ^{204}Pb is mostly below detection limit. The average ^{204}Pb concentration is 3.5 ppb in olivine, and 5.4 ppb in mesostasis. These two minerals are the main hosts of non-radiogenic Pb, containing of ca. 77% and 23% of the total budget (estimated from abundances of these minerals, and average ^{204}Pb concentrations).

The Pb isotopic ratios in all minerals analysed by SIMS are not precise enough to quantify the contributions of radiogenic and non-radiogenic Pb components. However, the relatively low (and relatively more precise) $^{207}Pb/^{206}Pb$ ratios in mesostasis indicate the presence of radiogenic Pb. These results are consistent with observation of Bollard et al. (2017) that mesostasis is the main host of U (and radiogenic Pb) in chondrules.

5. DISCUSSION

5.1. Efficiency of the step leaching procedure in case of omnipresent non-radiogenic Pb

Three different protocols were applied to the mega-chondrule A25-2 fractions: a five-step protocol was used for the four A31 fractions, a ten-step for the three A66 fractions, and a 12-13 steps for the two A68 fractions. All fractions processed with the same protocol tend to yield similar trends of $^{206}Pb/^{204}Pb$ ratios that is an overall increase of the $^{206}Pb/^{204}Pb$ ratios through the leaching procedure (Fig. 6). The first HF steps (1M HF) tend to have higher $^{206}Pb/^{204}Pb$ ratios than the final residues. This has been observed in both single and multi-chondrules fractions from Allende (Connelly and Bizzarro, 2009). Regardless of the protocol, a significant amount of Pb with a terrestrial composition is released during the first steps of leaching up to the 0.5 M HNO_3 step (Fig. 6). These observations confirm the efficacy of the step-leaching procedure in separating Pb components present in chondrules, although its efficiency can depend on a number of factors.

404 The observed patterns of Pb, U and Th release, as well as $^{206}Pb/^{204}Pb$ ratios through the
405 different steps of the leaching protocols (Fig. 6) reflect the abundances of the different
406 mineral phases present in the A25-2 megachondrule (olivine, clinopyroxene, mesostasis and
407 spinel) and their content of U, Th and radiogenic and non-radiogenic Pb revealed by the
408 SIMS analyses. The presence of a terrestrial Pb component in various leaching steps (Fig. 6)
409 complicates interpretation of effects of the grain size, the nature and strength of acids used for
410 the leaching steps and the number of steps required.

411 The proportion of total Pb content released during each step of the leaching procedure
412 follows a trend for each protocol applied with some differences between the fractions. In the
413 batch A31, the largest amount of Pb in fine and medium fractions is released in the 0.1 M
414 HBr step. The coarse fraction released a larger quantity of Pb during the later dissolution
415 steps. The $^{206}Pb/^{204}Pb$ ratios of the 0.1 M HBr leaching step in fine fractions that are close to
416 the modern terrestrial value (Stacey and Kramers 1975) suggest that Pb from terrestrial
417 contamination is more efficiently removed with 0.1 M HBr if the grain size is smaller (Fig.
418 6). In subsequent leaching steps, the Pb isotopic composition gradually becomes more
419 radiogenic.

420 Fractions in the batch A66 show a more complex pattern of Pb release during leaching,
421 and greater variations between the fractions. The general trend is, however, similar: most Pb
422 from fine and medium fractions is released during the early leaching steps (up to 0.02 M HBr,
423 Fig 6), while the coarse fraction retains Pb more strongly, and releases it in more
424 concentrated and hotter acids (at the 0.5 M HNO_3 and 6 M HCl steps, Fig. 6). The $^{206}Pb/^{204}Pb$
425 ratio in the fine fraction gradually increases through leaching (although drops in the residue),
426 whereas the $^{206}Pb/^{204}Pb$ variations in medium and coarse fractions are more erratic.

427 The two fractions of the batch A68 show an overall increase of both Pb amounts and
428 $^{206}Pb/^{204}Pb$ ratios, through the entire leaching sequence up to the diluted HF steps regardless
429 of the grain size (Fig. 6).
430 Considering that most Pb is released during the earliest acid leaching steps (up to 0.02
431 and 0.1M HBr), and this Pb has an isotopic composition close to terrestrial Pb, as well as the
432 absence of easily acid soluble minerals in the megachondrule A25-2, we interpret these
433 observations as indicating that terrestrial Pb was most abundant, and most labile, in cracks,
434 joints between mineral grains, and at the surface of the fragments.
435 Furthermore, faster leaching protocols such as used for the batch A31 produce noticeable
436 differences between fine and coarse fractions in elemental and isotopic distributions between
437 the leaching steps, while in the slower protocols (batch A68) this difference almost
438 disappears. This observation suggests that the step leaching occurs under non-equilibrium
439 conditions, and the efficiency of Pb component separation is influenced by kinetics of
440 mineral dissolution.
441
442 **5.2. Efficiency of acid leaching steps to yield data suitable for Pb-Pb isochron age**
443 **determination**
444 In the materials that contain sufficiently radiogenic Pb, the efficiency of removal of other
445 Pb components by acid leaching steps is assessed primarily by the increase of $^{206}Pb/^{204}Pb$
446 ratio, which reflects increasing ratio of radiogenic Pb relative to non-radiogenic Pb. This
447 criterion is, however, inadequate for materials that contain two or more resilient non-
448 radiogenic Pb components. In order to produce data suitable for age determination, the step
449 dissolution procedure should be able to reduce a multi-component mixture to a binary
450 mixture of in-situ grown radiogenic Pb and a single non-radiogenic component with
451 homogeneous isotopic composition. This is particularly critical for the A25-2 mega-

chondrule for which up to 85% of the total Pb content present in a given fraction is removed during the first steps of the leaching procedure (water+acetone and HBr) and yields rather unradiogenic Pb ratios.

The initial goal of this study was to construct a precise and statistically robust isochron for the mega-chondrule A25-2 containing at least some highly radiogenic data. However, since we could not obtain highly radiogenic points, we opted for a lesser goal of constraining a meaningful binary mixture of radiogenic Pb with significant, but variable, amount of non-radiogenic Pb. The points that were deemed not fitting the two-component model have to be removed to produce a reliable isochron.

The data evaluation and filtering process applied to the megachondrule A25-2 dataset involves several successive steps of isochron regressions and model-date calculations and is summarised in Table 5. The complete set of isochron and model-date plots, the table with the data used in the calculations and plots, as well as the list of points included in each regression, are presented in supplementary material (EA-dataset 5).

As the entire dataset fails to yield a statistically robust isochron (regression 1; Fig. R1 in EA-dataset 5), the dataset was first screened for the amount of contamination Pb. The Pb released by the first leachates: water + acetone, dilute HBr, and 0.5 M HNO_3, is dominated, or heavily affected, by terrestrial contamination as was shown earlier (Fig. 6). Therefore, these leachates were not considered for the isochron construction (regression 2; Fig. R2 in EA-dataset 5). As the measured Pb blanks range from 0.5 pg to 1.6 pg, in the next filtering step (regression 3; Fig. R3 in EA-dataset 5) the fractions that contain less than 4 pg of ^{206}Pb have been removed. These fractions are most affected by blank uncertainty (Connelly et al, 2017) and are less precise than the other data (see data table in EA-dataset 5). Removal of very small fractions is, however, inconsequential for the regression quality. In the next step (regression 4; Fig. R4 in EA-dataset 5), three analyses with extreme U-Pb discordance

>500% were removed. These data also display low $^{206}Pb/^{204}Pb$ ratios (see EA-5 in Supplementary Material). Such an extreme discordance points to the open system behaviour that is likely to involve gain and/or loss of the parent and daughter atoms, as well as addition of contaminant Pb. This filtering step considerably reduced the data dispersion (MSWD is reduced from 382 to 18) and increased precision (from ±23 Ma to ±5.2 Ma; Fig. R4 in EA-dataset 5).

In the remaining set of 30 points, the 11 fractions produced by leaching steps in 2.5 M HCl and hot 6–7 M HCl and HNO_3 yielded the lowest model dates between 4542-4562 Ma (Fig. R4b in EA-dataset 5), which suggests the presence of a small remaining amount of terrestrial contamination. Elimination of these points leaves a data set of 19 analyses that consists of three residues from the batch A31, one residue from the batch A66, and all HF leaching steps. A regression of these data (regression 5; Fig. R5 in in EA-dataset 5) yields the isochron date of 4567.5±4.1 Ma, MSWD=7.2 that passes through the isotopic composition of primordial Pb (Fig. R5c in EA-dataset 5).

To evaluate the cause of the remaining data dispersion, the $^{207}Pb^*/^{206}Pb^*$ model dates calculated from these analyses are plotted in the sequence of leaching steps (Fig. 7). For each of the five mineral fractions that were leached with HF (A66-108, -111, -121, A68-3, -12), the model dates increase from the earlier to the later leaching steps, and reach the values of 4571-4572 Ma, distinctly older than the accepted age of Solar System. These variations closely resemble leaching-induced isotopic fractionation (Amelin et al., 2016) that has been observed in highly radiogenic systems. The variations between the HF leaching steps are similar in magnitude, and are induced by the same treatment. These variations are not caused by the difference between assumed and real initial Pb isotopic composition, as in the latter case the model dates would have been correlated with the $^{206}Pb/^{204}Pb$ ratios, but in fact no

such correlation exists. Therefore, we suggest that these variations are related to isotopic fractionation during the HF leaching steps.

5.3. $^{207}Pb/^{206}Pb$ variations related to leaching-induced fractionation of radiogenic Pb

To negate the detrimental effect of this leaching-induced fractionation, the data for HF leachates (fractions A66-111, A66-121, A68-3 and A68-12) and for HF leachates and residue for fractions A66-108, were numerically re-combined. The resulting dataset includes five re-combined fractions and three residues from the batch A31 (i.e. the same set of data as in regression 5 but with re-combination of HF leachates) and yields an isochron date (regression 6: Fig. R6 in EA-dataset 5) of 4564.5±7.7 Ma (MSWD=5.1). This date is not statistically robust as the regression involves a significant excess dispersion of points as expressed by the MSWD higher than 2. Nevertheless, this imperfect regression appears to pass through the isotopic composition of primordial Pb (Fig. R6a in EA-dataset 5). A plot of model dates for that data set shows that the three residue analyses from the batch 31 yield lower $^{207}Pb^*/^{206}Pb^*$ dates than re-combined fractions (Fig. R6b in EA-dataset 5). Considering shorter leaching procedure used in the batch A31, we interpret this observation as evidence for the presence of small residual terrestrial contamination in the A31 residues. By eliminating them from isochron regression in the final step for filtering out terrestrial Pb component, the resulting regression (regression 7: Fig. 8 and Figs. R7a,b and c in EA-dataset 5) using the five re-combined fractions yields an isochron without statistically significant excess scattering that corresponds to the age of 4568.5±3.0 Ma, MSWD=1.6, probability of fit 0.20.

5.4. Step leaching protocols for future chondrule dating?

525 Multi-step leaching in a variety of acids of increasing concentration and temperature thus
526 allowed complete, or almost complete, removal of terrestrial Pb from the mega-chondrule
527 A25-2, bringing it closer to a binary mixture of radiogenic and initial Pb that is suitable for
528 age determination. Gradually decreasing amounts of terrestrial Pb were present in most
529 leaching steps, and were finally reduced to an insignificant level by leaching in hot
530 concentrated HNO_3 and HCl, although in the samples processed with shorter leaching
531 procedure (batch A31), traces of terrestrial Pb still could be detected even in the residues. All
532 HF leaching steps in batches A66 and A68 that were applied after HBr, HNO_3 and HCl
533 washing appear to be free from terrestrial contamination, but appear to be affected by
534 leaching-induced fractionation of radiogenic ^{206}Pb and ^{207}Pb. Fortunately this fractionation
535 can be cancelled by numeric re-mixing of the leaching steps. Despite isotopic fractionation
536 induced by leaching in HF, we consider application of multiple leaching steps in HF of
537 increasing concentration essential for confirmation of complete removal of the terrestrial
538 component. In a general way, this study shows that protocols with a longer sequence of
539 leaching are more suitable for objects where terrestrial contamination is stubborn.

540 Nevertheless, only limited separation of radiogenic and initial Pb was achieved during
541 step leaching. This may be related to the mineralogy of the mega-chondrule A25-2 that is
542 dominated by olivine which essentially is free of U and Pb, while the chondrule mesostasis
543 and to a lesser extend the clinopyroxene are the main hosts of both radiogenic and initial Pb,
544 as also shown by the SIMS analyses, and are the main contributors to the Pb-Pb isochron.

545 Can this study advise us about the chondrule mineralogy that is most favourable for
546 precise Pb-isotopic dating, and what dissolution procedures would make the best use of this
547 mineralogy? This important question is mostly beyond the scope of this study. Answering it
548 would require determination of the mineral-scale distribution of U, Th and radiogenic and
549 non-radiogenic Pb isotopes in several chondrules with varying mineralogy and content of

550 non-radiogenic Pb, combined with leaching experiments on the same chondrules. Still, we
551 can present some speculations about the chemical protocol that is likely to work for barred
552 olivine chondrules. Such a protocol would involve washing the chondrule with the different
553 acids followed by full dissolution with concentrated HF. This procedure would have the
554 advantage of removing efficiently terrestrial Pb and avoiding Pb fractionation during
555 different HF steps. However, this procedure would only be applicable to large chondrules that
556 can be split into several fractions to yield enough data for isochron construction of sufficient
557 precision.

558 SIMS analyses of the mega-chondrule A25-2 showed that the mesostasis and
559 clinopyroxene are the main hosts of U but also contain non-radiogenic Pb. The presence of
560 mineral phases containing such a Pb component does not make a chondrule unsuitable for
561 construction of an isochron. Non-radiogenic Pb was detected at low levels in all minerals in
562 six chondrules from H5 chondrite Richardton (Amelin et al. 2003), which did not prevent
563 their successful U-Pb dating (Amelin et al. 2005). Furthermore, most chondrules have
564 mineralogy similar as those of the mega-chondrule A25-2 (Krot et al., 2009) yet have also
565 been successfully dated (Amelin et al. 2002, Amelin and Krot 2007, Connelly et al., 2012;
566 Bollard et al., 2017). Apparently, some yet unrecognized microstructural peculiarity of the
567 mega-chondrule A25-2 made it unusually retentive of both initial Pb and contaminant Pb.
568

569 **5.5. Isotopic composition of Pb in the Allende matrix**

570 Since all analysed fractions of the mega-chondrule A25-2 that are available for age
571 determination contain substantial amounts of initial Pb, construction of a meaningful isochron
572 requires comprehensive characterisation of initial Pb, and other possible non-radiogenic Pb
573 components. Along with primordial Pb that is deduced from the isotopic composition of Pb in
574 U-free troilite nodules in iron meteorites and terrestrial contamination, chondrules can

575 contain Pb transferred from the matrix during a metamorphic, metasomatic or impact event.
576 The presence of high-Ca pyroxene crystals in chondrule mesostasis and sodium-rich nature
577 for the latter provide evidence for a moderate thermal metamorphism associated with iron-
578 alkali metasomatism occurring after aggregation of the Allende meteorite (Krot et al., 1995,
579 1998). Therefore, Pb migration from the Allende matrix to the mega-chondrule A25-2 is
580 plausible. Measurement of the Pb isotopic composition of the matrix can help detect such a
581 component.

582 There is a drastic difference between Pb isotopic systematics of matrix powders and
583 fragments (Fig. 5a). Three data points of matrix powders plot along the line between
584 primordial Pb and modern terrestrial crustal Pb. These powder fractions clearly contain
585 significant contamination, most likely introduced during crushing.

586 The Pb-isotopic data for the matrix-fragment fractions consist of individually selected
587 matrix fragments that are visually devoid of CAI and chondrule materials. They were
588 ultrasonically cleaned from dusty particles and surface contamination (Fig. 5b) and are quite
589 different in terms of their Pb-Pb systematics. One point (A116-4) plots closer to the line
590 connecting primordial Pb and modern terrestrial crustal Pb, probably due to a small amount
591 of contamination with Pb having a similar isotopic composition to that present in the
592 powders. Six other fragment fractions form a linear array that yields a regression that passes
593 between the estimates of primordial Pb from Tatsumoto et al. (1973) and Blichert-Toft et al.
594 (2010), and show no detectable signs of terrestrial contamination.

595 An isochron regression of the six analyses of fragment fractions yields the date of
596 4606±29 Ma (MSWD = 0.42, probability of fit: P = 0.79). The younger age limit of the
597 matrix isochron at 95% confidence level is 4577 Ma, or 10 Ma older than the best estimate of
598 the time of formation of the CAIs and, by inference, the age of the Solar System
599 (4567.3±0.16 Ma; Connelly et al., 2012). This anomalously old apparent isochron date of the

matrix could be related to the presence of pre-solar grains, and/or capture by the matrix minerals of radiogenic Pb released from CAIs and chondrules early in the history of the parent asteroid (Amelin 2008). Since the matrix is a mixture of various minerals, both presolar and those formed in the solar protoplanetary disk, that have various ages and $^{238}U/^{235}U$ ratios, we suggest that the date yielded by the matrix fragment isochron does not correspond to any specific natural event.

5.6. The Pb-Pb isochron for the mega-chondrule A25-2 – how reliable?

5.6.1. Unconstrained vs. constrained regression to assumed initial Pb composition

The isochron for five re-combined HF leaching fractions (regression 7; Table 5 and Fig. 8) yields the age of the mega-chondrule A25-2 of 4568.5±3.0 Ma (MSWD=1.6, probability of fit 0.20). The relatively large uncertainty is a result of a small spread of $^{204}Pb/^{206}Pb$ due to co-existence of initial and radiogenic Pb in the main carrier of U and radiogenic Pb: the chondrule mesostasis. It may be tempting to try to improve precision of the age by including the data point of initial Pb, and thereby expanding the span of the data, if the exact identity of initial Pb in the mega-chondrule could be determined. It is commonly assumed (whether correctly or not) that the initial Pb in the earliest Solar System materials: CAIs, chondrules, and the most ancient achondrites, corresponds to the composition of primordial Pb determined from analysis of U-free troilite nodules in iron meteorites. In Figure 8b, the projection of the isochron for the mega-chondrule re-combined fractions (regression 7) is compared to the isotopic composition of primordial Pb as estimated by Tatsumoto et al. (1973) and Blichert-Toft et al. (2010), and the analyses of matrix fragments. The Pb isotopic composition of the Canyon Diablo troilite CDT of Tatsumoto et al. (1973) plots within the 95% uncertainty envelope of the isochron, but the more precise, and analytically more rigorous estimate of primordial Pb by Blichert-Toft et al. (2010) or similar value from

625 Connelly et al. (2008b), as well as the analyses of the matrix, are outside the 95% confidence
626 uncertainty envelope. The residual non-radiogenic Pb in the re-combined HF leachates is
627 therefore close to, but not identical, to the current best estimate of the Solar System's
628 primordial Pb (as established by Blichert-Toft et al., 2010 and Connelly et al., 2008b).
629 Therefore, including either primordial Pb, or the matrix analyses in the chondrule regression,
630 is not justified despite the opportunity to gain up to four times improvement in the age
631 precision (regressions 8 to 11 in Table 5; Figs R8, R9, R10 and R11 in EA-dataset 5).
632 Regressions using the same dataset and constrained to CDT and Allende matrix yield ages
633 distinct by only 0.06 Myrs (Figs. R8 and R11 in EA-dataset 5). Nevertheless, we consider the
634 unconstrained isochron age of 4568.5±3.0 Ma the best estimate of the age of the mega-
635 chondrule A25-2.
636
637 *5.6.2. Assessing the reliability of the isochron*
638 The validity of this isochron can be estimated using six criteria that Connelly et al.
639 (2017) formulated for assessment of quality of Pb-Pb isochrons generated by stepwise
640 dissolution of meteorite materials such as chondrules. These criteria are:
641 1) The data must define a statistically valid linear array (MSWD ≤ 2, probability of
642 fit ≥ 0.05).
643 2) The number of analyses defining an isochron should exceed those rejected.
644 3) The amount of Pb analysed in at least a subset of fractions should be large
645 enough to be relatively insensitive to the blank correction.
646 4) The data array should be checked for evidence of mass independent fractionation
647 that could compromise the calculated radiogenic $^{207}Pb/^{206}Pb$.

5) If there is initial Pb present in the sample, the back projection of the isochron to non-radiogenic Pb should point to a composition consistent with the earlier history of the sample or its precursor material.
6) For any sample modelled as being free of initial Pb, the back projection of the isochron to non-radiogenic Pb should point to an isotopic composition that is consistent with modern terrestrial Pb.

Our isochron for five re-combined HF leaching fractions satisfies criteria 1, 3, 4 and, with some reservations, agrees with criterion 5. In the context of this study, the criterion 6 is irrelevant. The criterion 2 that the number of analyses defining an isochron should exceed the number of rejected points, however, appears severely violated due to extensive filtering to eliminate terrestrial contamination. We argue nonetheless that, while this criterion is generally sensible and useful for evaluation of sufficiently radiogenic Pb-isotopic data sets, there are cases where its violation is inevitable and/or justifiable. The analyses of the mega-chondrule A25-2 in this study is one of these cases. The regression is based on re-combination of 16 analyses, or 23% of the total number of 69, which seems to be a small fraction. However, the very first filtering step eliminates 28 analyses of the earliest leaching steps (water+acetone and HBr steps) that were designated for removal of the most conspicuous terrestrial contamination. In many studies, such leachates would have been discarded without analysis. In this study, they were analysed only to observe the dynamics of de-contamination, without any intent of including them into the isochron age determination. The next two filtering steps eliminated (1) very small leachates prone to blank uncertainty that is a valid analytical filter following the criterion #3 of Connelly et al. (2017), and (2) leachates with extreme U-Pb discordance suspect for an open system behaviour that we consider a valid geochemical filter. The number of fractions left after these filtering steps is 30, and more than half of them were used in construction of the final isochron.

673 Our data filtering process was based on geochemical and analytical criteria, and does not
674 require statistical filters, let alone arbitrary cherry-picking of data points. We therefore
675 suggest that the formal violation of criterion #2 of Connelly et al. (2017) did not compromise
676 the accuracy of the age in this case.
677

678 **5.7. Implications of the U-Pb age of the mega-chondrule A25-2**

679 Our preferred interpretation of the 4568.5±3.0 Ma isochron age is that it accurately
680 (within its uncertainty limits) reflects of the time of the mega-chondrule formation. The way
681 from the raw data set to this age involved very extensive manipulation of data. No stand-
682 alone analyses were used in the final age calculation. This is an inevitable result of our
683 interpretation of the variable dates in HF leaching steps as a being produced by leaching-
684 induced isotopic fractionation. While we believe that our choices in data filtering and
685 recombination are the best possible, this level of data manipulation necessarily makes the age
686 more model-dependent than the ages obtained by direct regressing of highly radiogenic data.
687 The latter are clearly preferred for construction of the Solar System timescale. Considering
688 significant model dependence of the age of the mega-chondrule A25-2, we suggest treating
689 the following discussion as tentative and potentially bearing an additional uncertainty from
690 the age model dependence.
691 The Pb-Pb age of the mega-chondrule A25-2 overlaps the average age of CAIs in CV
692 chondrites, and the ages of the oldest single chondrules from the Allende and L3 chondrites
693 (Connelly et al., 2012; Bollard et al., 2017; Fig. 9). It is, however, distinctly older (at its
694 lower limit of 4565.5 Ma at 95% confidence level) than the fractions of multiple Allende
695 chondrules analysed by Connelly et al. (2008) and Connelly and Bizzarro (2009). These two
696 ages of 4564.46±0.45 Ma and 4564.33±0.81 Ma (Fig. 9, recalculated using the average
697 $^{238}U/^{235}U$ ratio from the analyses of pooled Allende chondrules; $^{238}U/^{235}U = 137.786±0.004$;

698 Brennecka et al., 2015) are clearly younger that those of the CV3 single chondrules (Fig. 9).
699 This suggests that these two dates were dominated by chondrules of a younger generation.
700 The age of Allende chondrules fractions of 4565.61±1.00 Ma of Amelin and Krot, 2007 (also
701 recalculated using $^{238}U/^{235}U$ of Brennecka et al. 2015) is, however, consistent with the age of
702 the mega-chondrule A25-2. In general, published Pb-isotopic data for pooled smaller
703 chondrules tend to be younger than the ages of individual larger chondrules, suggesting a
704 possible correlation between the size and age of Allende chondrules as recently proposed by
705 Bollard et al. (2019).

706 We, therefore, suggest that large and small chondrules might have formed by two
707 different thermal events, which could involve similar or different mechanisms of chondrule
708 formation. Larger chondrules have been formed by a more energetic event than those that
709 formed the smaller ones. Alternatively, both large and small chondrules could have been
710 formed during the same continuous thermal event, but the large chondrules formed when this
711 event reached its maximum intensity around 4567 Ma, then the intensity decreased
712 progressively, yielding enough energy to produce only small chondrules. Nevertheless, this
713 interpretation should be considered with caution as it is based on a small number of ages of
714 individual chondrules.

715 The average model $^{232}Th/^{238}U$ ratio ($\kappa = 4.0 \pm 0.2$, 2σ) calculated from the radiogenic
716 $^{208}Pb^*/^{206}Pb^*$ ratios and $^{207}Pb/^{206}Pb$ model dates in the mega-chondrule A25-2 is similar,
717 within uncertainties, to the value calculated from Pb isotopic composition of troilites ($\kappa =$
718 3.876 ± 0.016; Blichert-Toft et al., 2010) and to the accepted values for the Solar System ($\kappa =$
719 3.77, Lodders, 2003, $\kappa = 3.9 \pm 0.2$; Rocholl and Jochum, 1993). It should be noted that two
720 Allende individual chondrules C30 and C20 analysed by Connelly et al. (2012), which are
721 among the oldest dated so far, yield the κ values of 4.4–4.5 that are only slightly higher than
722 κ value calculated for the mega-chondrule A25-2 and relatively close to the average solar

723 value. The κ values in CAIs (5.5–7.8, Jacobsen et al., 2008) are significantly higher than in
724 all studied chondrules. These observations suggest that, despite having the same age, Allende
725 CAIs and the oldest chondrules either formed in different reservoirs, or experienced different
726 mechanisms of fractionation between U and Th. These possibilities are not mutually
727 exclusive. It is likely that the higher temperature that was required for CAI formation caused
728 Th/U fractionation by partial volatilisation of U, whereas the temperature during chondrule
729 formation was not high enough to volatilise U, thereby causing chondrules to have Th/U
730 ratios close to the bulk Solar System values.

731 **5.8. Comparison between Pb-isotopic and Al-Mg ages.**

732 The $(^{27}Al/^{26}Al)_0$ ratio of the mega-chondrule A25-2 is $(5.4\pm6.5)\times10^{-6}$. Assuming uniform
733 distribution of ^{26}Al with canonical initial $(^{27}Al/^{26}Al)_0$ (Jacobsen et al. 2008), the data
734 corresponds to a mega-chondrule age of 4565.0+0.8/-∞, relative to the age of 4567.3± 0.16
735 Ma that is CAI formation (Connelly et al. 2012). The difference between the Pb-isotopic age
736 of mega-chondrule of 4565.5 Ma and the ^{26}Al-^{26}Mg age assuming uniform ^{26}Al distribution at
737 "canonical" level is 3.5±3.1 Ma. Using instead the initial $(^{27}Al/^{26}Al)_0$ of $(1.36\pm0.72)\times10^{-5}$
738 proposed by Bollard et al. (2019) for the chondrule-forming region yields the ^{26}Al-^{26}Mg age
739 for the mega-chondrule of 4566.4+0.8/-∞, and the difference between Pb-isotopic and ^{26}Al-
740 ^{26}Mg ages of 2.1±3.1 Ma. This age overlaps the preferred value of the Pb-isotopic age. Our
741 Pb-Pb and Al-Mg data of the mega-chondrule A25-2 are, therefore, inconsistent with the
742 hypothesis of an uniform distribution of ^{26}Al in the solar protoplanetary disk. Our data agree
743 with the difference in initial $(^{27}Al/^{26}Al)_0$ between CAI and chondrule forming regions that
744 was suggested by Bollard et al. (2019).
745

746 **6. Conclusions**

747 The mega-chondrule A25-2, a rare, very large chondrule in the Allende meteorite proved
748 to be a difficult object to date. It contained a significant amount of terrestrial Pb and almost
749 inseparable radiogenic and initial Pb. Despite these difficulties, our study using three
750 different leaching protocols consisting of multiple leaching steps using water, acetone, HBr,
751 HCl, HNO_3 and HF allowed us to reduce the complex three-component Pb isotopic mixture
752 to a binary mixture of radiogenic and initial Pb that yielded a reasonably reliable, even if
753 relatively imprecise and model-dependent, Pb-isotopic age of 4568.5±3.0 Ma, supported by
754 directly measured $^{238}U/^{235}U$. The ^{26}Al-^{26}Mg study yielded $^{27}Al/^{26}Al$ ratio of $(5.4\pm6.5)\times10^{-6}$ at
755 the time of the mega-chondrule formation. An agreement between the Pb-isotopic and Al-Mg
756 ages is achieved using the initial $^{27}Al/^{26}Al$ in the chondrule formation region proposed by
757 Bollard et al. (2019), but not using the canonical value.
758 The age of this chondrule suggests that it belongs to the older generation of Allende
759 chondrules that formed over the period of time overlapping formation of CAIs. Its model
760 $^{232}Th/^{238}U$ derived from Pb-isotopic systematics is indistinguishable from the bulk Solar
761 System value, suggesting the lack of volatility-related Th/U fractionation in the region of the
762 solar protoplanetary disk where this chondrule formed.
763 Analyses of the Allende matrix that were intended to verify the isotopic composition of
764 initial Pb in the mega-chondrule A25-2 confirmed the composition of the initial Pb close to
765 the current best estimate of the primordial Pb of the Solar System, but yielded an isochron
766 corresponding to the age of 4606±29 Ma that exceeds the age of the Solar System. This
767 anomalously old apparent date can be related to the presence of pre-solar grains, and/or an
768 early transfer of radiogenic Pb from CAIs and chondrules, and probably does not correspond
769 to any specific event.
770
771 **Acknowledgements**

We thank Dr. J. Connelly, an anonymous reviewer, and associated editor Dr. C. Herd for their constructive and helpful comments and editorial handling this paper. We are grateful to S. Zink for analytical support of the SPIDE^{2}R lab at the ANU, and to Prof. Vickie Bennett for her continuing support that made this work possible. This work was supported through NASA Grants NNX14AM62G and NNX16AD34D to Q.-Z.Y., and NNX17AE22G to A.N. Krot.

References

Amelin, Y., Stern, R. A. and Krot, A. N. (2003). Distribution of U, Th, Pb and Nd between minerals in chondrules and CAIs. *Lunar and Planetary Science* **XXXIV**, #1200.

Amelin, Y., Ghosh, A., Rotenberg, E. (2005) Unraveling the evolution of chondrite parent asteroids by precise U–Pb dating and thermal modeling. *Geochim. Cosmochim. Acta* **69**, 505–518.

Amelin, Y. (2006) The prospect of high-precision Pb isotopic dating of meteorites. *Meteorit. Planet. Sci.* **41**, 7–17.

Amelin Y. (2008) The U–Pb systematics of angrite Sahara 99555. *Geochim. Cosmochim. Acta* **72**, 4874–4885.

Amelin Y., Krot A. N., Hutcheon I. D. and Ulyanov A. A. (2002) Lead isotopic ages of chondrules and calcium–aluminum–rich inclusions. *Science* **297**, 1678–1683.

Amelin Y. and Davis W. J. (2006) Isotopic analysis of lead in subnanogram quantities by TIMS using a ^{202}Pb-^{205}Pb spike. *J. Analyt. Atomic Spectrom.* **21**, 1053–1061.

Amelin Y. and Krot A. N. (2007) Pb isotopic age of the Allende chondrules. *Meteorit. Planet. Sci.* **42**, 1321–1335.

796 Amelin Y., Connelly J., Zartman R. E., Chen J. H., Göpel C. and Neymark L. A. (2009)
797 Modern U–Pb chronometry of meteorites: advancing to higher time resolution reveals new
798 problems. *Geochim. Cosmochim. Acta* **73**, 5212–5223.
799 Amelin Y., Kaltenbach A., Iizuka T., Stirling C. H., Ireland T. R., Petaev M. and
800 Jacobsen S. B. (2010) U–Pb chronology of the Solar System's oldest solids with variable
801 ^{238}U–^{235}U. *Earth Planet. Sci. Lett.* **300**, 343–350.
802 Amelin Y., Yin Q.-Z., Koefoed P., Merle R., Huyskens M. and Iizuka T. (2016)
803 Fractionation of radiogenic Pb isotopes induced by acid leaching: a pervasive phenomenon in
804 Pb-isotopic dating of meteorites. In: Goldschmidt Conference Abstracts **57**.
805 Arden J. W. and Cressey G. (1984) Thallium and lead in the Allende CV3 carbonaceous
806 chondrite. A study of the matrix phase. *Geochim. Cosmochim. Acta* **48**, 1899–1912.
807 Asphaug E., Jutzi M., and Movshovitz N. (2011) Chondrule formation during
808 planetesimal accretion. *Earth Planet. Sci. Lett.* **308**, 369–379.
809 Blichert-Toft J., Zanda B., Ebel D. S. and Albarède F. (2010) The Solar System
810 primordial lead, *Earth Planet. Sci. Lett.* **300,** 152-163.
811 Bizzarro M., Baker J. A. and Haack H. (2004) Mg isotope evidence for contemporaneous
812 formation of chondrules and refractory inclusions. *Nature* **431**, 275–278.
813 Bollard J., Connelly J. N., Whitehouse M. J., Pringle E. A., Bonal L., Jørgensen J. K.,
814 Nordlund Å., Moynier F. and Bizzarro M. (2017) Early formation of planetary building
815 blocks inferred from Pb isotopic ages of chondrules. *Science Advances* **3**, e170040.
816 Bollard J., Connelly J. N. and Bizzarro M. (2015) Pb-Pb dating of individual chondrules
817 from the CBa chondrite Gujba: Assessment of the impact plume formation model. *Meteorit.*
818 *Planet. Sci.* **50**, 1197–1216.
819 Bollard J., Kawasaki N., Sakamoto N., Olsen M., Itoh S., Larsen K., Wielandt D.,
820 Schiller M., Connelly J. N., Yurimoto H., Bizzarro M. (2019) Combined U-corrected Pb-Pb

821 dating and ^{26}Al-^{26}Mg systematics of individual chondrules – Evidence for a reduced initial
822 abundance of ^{26}Al amongst inner Solar System chondrules. *Geochim. Cosmochim. Acta* **260**,
823 62–83.

824 Bonal L., Quirico E., Bourot-Denise M. and Montagnac G. (2006) Determination of the
825 petrologic type of CV3 chondrites by Raman spectroscopy of included organic matter.
826 *Geochim. Cosmochim. Acta* **70**, 1849–1863.

827 Bouvier A., Brennecka G. A. and Wadhwa M. (2011) Absolute chronology of the first
828 solids in the Solar System. *Workshop on the Formation of the First Solids in the Solar*
829 *System.*

830 Bouvier A. and Wadhwa, M. (2010) The age of the Solar System redefined by the oldest
831 Pb–b age of a meteoritic inclusion. *Nature Geoscience* **3**, 637–641.

832 Bouvier A., Blichert–Toft J., Moynier F., Vervoort J. D. and Albarède F. (2007) Pb–Pb
833 dating constraints on the accretion and cooling history of chondrites. *Geochim. Cosmochim.*
834 *Acta* **71**, 1583–1604.

835 Bouvier A., Wadhwa M. and Janney P. (2008) ^{26}Al–^{26}Mg and ^{207}Pb–^{206}Pb systematics in
836 an Allende inclusion. *71st Annual Meteoritical Society Meeting*. #5299 (abstr.).

837 Brennecka G. A., Budde G. and Kleine T. (2015) Uranium isotopic composition and
838 absolute ages of Allende chondrules. *Meteorit. Planet. Sci.* **50**, 1995–2002.

839 Brennecka G. A., Weyer S., Wadhwa M., Janney P. E., Zipfel J. and Anbar A. D. (2010)
840 ^{238}U/^{235}U variations in meteorites: Extant ^{247}Cm and implications for Pb-Pb dating. *Science* **327**,
841 449–451.

842 Budde G., Kleine T., Kruijer T. S., Burkhardt C. and Metzler K. (2016) Tungsten
843 isotopic constraints on the age and origin of chondrules. *Proc. National Acad. Sci.* **113**,
844 2886–2891.

845 Chen J. H. and Tilton G. R. (1976) Isotopic lead investigations on the Allende
846 carbonaceous chondrite. *Geochim. Cosmochim. Acta* **40**, 635–643.
847 Cody G. D., Alexander C. M. O. D., Yabuta H., et al. (2008) Organic thermometry for
848 chondritic parent bodies. *Earth Planet. Sci. Lett.* **272**, 446–455.
849 Connelly J., Amelin Y., Krot A. N. and Bizzarro M. (2008a). Chronology of solar
850 system's oldest solids. *Astrophys. J. Letters* **675**, L121–L124.
851 Connelly J. N., Bizzarro M., Thrane K., Baker J.A. (2008b) The Pb–Pb age of Angrite
852 SAH99555 revisited. *Geochim. Cosmochim. Acta* **72**, 4813–4824.
853 Connelly J. N. and Bizzarro M. (2009) Pb–Pb dating of chondrules from CV chondrites
854 by progressive dissolution. *Chem. Geol.* **259**, 143–151.
855 Connelly J. N., Bizzarro M., Krot A. N., Nordlund Å., Wielandt D. and Ivanova M. A.
856 (2012) The absolute chronology and thermal processing of solids in the solar protoplanetary
857 disk. *Science* **338**, 651–655.
858 Connelly J. N., Bollard J., Bizzarro M. (2017) Pb–Pb chronometry and the early Solar
859 System. *Geochim. Cosmochim. Acta* **201**, 345–363.
860 Dauphas N. and Chaussidon M. (2011) A perspective from extinct radionuclides on a
861 young stellar object: the Sun and its accretion disk. *Annual Rev. Earth Planet. Sci.* **39**,
862 351–386.
863 Desch S. J. and Connolly H. C. Jr. (2002) A model of the thermal processing of particles
864 in solar nebula shocks: Application to the cooling rates of chondrules. *Meteorit. Planet. Sci.*
865 **37**, 183–207.
866 Desch, S. J., Ciesla F. J., Hood L L. and Nakamoto T. (2005) In Chondrites and the
867 Protoplanetary Disk, vol. 341 (eds. A. N. Krot, E. R. D. Scott and B. Reipurth). ASP
868 Conference Series, 849–873.

869 Davis A. M., Richter F. M., Mendybaev R. A., Janney P. E., Wadhwa M. and McKeegan
870 K. D. (2005) Isotopic mass fractionation laws and the initial solar system $^{26}Al/^{27}Al$ ratio.
871 *Lunar Planet. Sci. XXXVIII*, Abstract #2334.
872 Guimon R. K., Symes S. J. K., Sears D. W. G. and Benoit P. H. (1995) Chemical and
873 physical studies of type 3 chondrites XII: The metamorphic history of CV chondrites and
874 their components. *Meteorit. Planet. Sci.* **30**, 704–714.
875 Hutcheon I. D. and Hutchison R. (1989) Evidence from the Semarkona ordinary
876 chondrite for Al–26 heating of small planets. *Nature* **337**, 238–241.
877 Huss G. R., MacPherson G. J., Wasserburg G. J., Russell S. S. and Srinivasan G. (2001)
878 Aluminum-26 in calcium–aluminum-rich inclusions and chondrules from unequilibrated
879 ordinary chondrites. *Meteorit. Planet. Sci.* **36**, 975–997.
880 Hutcheon I. D., Marhas K. K., Krot A. N., Goswami J. N. and Jones R. H. (2009) ^{26}Al in
881 plagioclase–rich chondrules in carbonaceous chondrites: Evidence for an extended duration
882 of chondrule formation. *Geochim. Cosmochim. Acta* **73**, 5080–5099.
883 Ito K.T.M., Hibiya Y., Homma Y., Mikouchi T., Iizuka T. (2019) The promise and
884 potential pitfalls of acid leaching for Pb-Pb chronology. *Chem. Geol.* **525**, 343–355.
885 Itoh S. and Yurimoto, H. (2003) Contemporaneous formation of chondrules and
886 refractory inclusions in the early Solar System. *Nature* **423**, 728-731.
887 Jacobsen B., Yin Q.-Z., Moynier F., Amelin Y., Krot A. N., Nagashima K., Hutcheon I.
888 D. and Palme H. (2008) ^{26}Al–^{26}Mg and ^{207}Pb–^{206}Pb systematics of Allende CAIs: Canonical
889 solar initial $^{26}Al/^{27}Al$ ratio reinstated. *Earth Planet. Sci. Lett.* **272**, 353–364.
890 Jones R. H., Grossman J. N. and Rubin A. E. (2005) Chemical, mineralogical and
891 isotopic properties of chondrules: Clues to their origin. In: *Chondrules and the*
892 *Protoplanetary Disk,* (eds. A. N. Krot, E. R. D. Scott and B. Reipurth), ASP Conference
893 Series **341**, Astronomical Society of the Pacific, San Francisco, 251–285.

894 Kawasaki N., Park C., Sakamotoc N., Park S. Y., Kim H. N., Kuroda M., Yurimoto H.
895 (2019) Variations in initial $^{26}Al/^{27}Al$ ratios among fluffy Type A Ca–Al-rich inclusions from
896 reduced CV chondrites. *Earth Planet. Sci. Lett.* **511**, 25–35.
897 Kita N. T., Nagahara H., Togashi S. and Morishita Y. (2000) A short duration of
898 chondrule formation in the solar nebula: Evidence from ^{26}Al in Semarkona ferromagnesian
899 chondrules. *Geochim. Cosmochim. Acta* **64**, 3913–3922.
900 Kita N. T., Huss G. R., Tachibana S., Amelin Y., Nyquist L. E., and Hutcheon I. D.
901 (2005) Constraints on the origin of chondrules and CAIs from short-lived and long-lived
902 radionuclides. In: *Chondrites and the protoplanetary disk* (eds. A. N. Krot, E. R. D. Scott and
903 B. Reipurth), ASP Conference Series, **341**. San Francisco, California: Astronomical Society
904 of the Pacific. pp. 558–587.
905 Kita N. and Ushikuto T. (2012) Evolution of protoplanetary disk inferred from ^{26}Al
906 chronology of individual chondrules. *Meteorit. Planet. Sci.* **47**, 1108–1119.
907 Kita N. T., Yin Q.–Z., Macpherson G. J., Ushikubo T., Jacobsen B., Nagashima K.,
908 Kurahashi E., Krot, A. N. and Jacobsen S.B. (2013) ^{26}Al–^{26}Mg isotope systematics of the first
909 solids in the early solar system. *Meteorit. Planet. Sci.* **48**, 1383–1400.
910 Krot A. N., Scott E. R. D., and Zolensky M. E. (1995) Mineralogical and chemical
911 modification of components in CV3 chondrites: Nebular or asteroidal processing? *Meteorit.*
912 *Planet. Sci.* ***30***, 748–775.
913 Krot A. N., Hutcheon I. D. and Keil K. (2002) Plagioclase–rich chondrules in the
914 reduced CV chondrites: Evidence for complex formation history and genetic links between
915 calcium-aluminum-rich inclusions and ferromagnesian chondrules. *Meteorit. Planet. Sci.* **37**,
916 155–182.

Krot A. N., Petaev M. I., Scott E. R. D., Choi B.-G., Zolensky M. E. and Keil K. (1998) Progressive alteration in CV3 chondrites: More evidence for asteroidal alteration. *Meteorit. Planet. Sci.* **33**, 1065–1085.

Krot A. N. Amelin Y., Bland P., Ciesla F. J., Connelly J., Davis A. M., Huss G. R., Hutcheon I. D., Makide K., Nagashima K., Nyquist L. E., Russell S. S., Scott E. R. D., Thrane K., Yurimoto H. and Yin Q.–Z. (2009) Origin and chronology of chondritic components: A review. *Geochim. Cosmochim. Acta* **73**, 4963–4997.

Krot A. N., Makide K., Nagashima K., Huss G. R., Ogliore R. C., Ciesla F. J., Yang L., Hellebrand E. and Gaidos E. (2012) Heterogeneous distribution of ^{26}Al at the birth of the solar system: evidence from refractory grains and inclusions. *Meteorit. Planet. Sci.* **47**, 1948–1979.

Krot A. N., Yurimoto H., McKeegan K. D., Leshin L., Chaussidon M., Libourel G., Yoshitake M., Huss G. R., Guan Y. and Zanda B. (2006) Oxygen isotopic compositions of chondrules: implication for understanding oxygen isotope evolution of the solar nebula. *Chem. Erde* **66**, 249–276.

Krot A. N., Nagashima K., Libourel G. and Miller K. E. (2018) Multiple mechanisms of transient heating events in the protoplanetary disk: Evidence from precursors of chondrules and igneous Ca,Al-rich inclusions. In: *Chondrules and the Protoplanetary Disk* (eds. S. S. Russell, H. C. Connolly Jr. and A. N. Krot), Cambridge University Press, pp. 11–56.

Kunihiro T., Rubin A. E., McKeegan K. D. and Wasson J. T. (2004) Initial ^{26}Al/^{27}Al in carbonaceous chondrite chondrules: Too little ^{26}Al to melt asteroids. *Geochim. Cosmochim. Acta* **68**, 2947–2957.

Kurahashi E., Kita N. T., Nagahara H. and Morishita Y. (2008) ^{26}Al–^{26}Mg systematics of chondrules in a primitive CO chondrite. *Geochim. Cosmochim. Acta* **72**, 3865–3882.

941 Larsen K., Trinquier A., Paton C., Schiller M., Wielandt D., Ivanova M., Connelly J.,
942 Nordlund A., Krot A. N. and Bizzarro M. (2011) Evidence for magnesium-isotope
943 heterogeneity in the solar protoplanetary disk. *Astrophys. J.* **735**, L37−L40.
944 Lee T., Papanastassiou D. A. and Wasserburg G. J. (1976) Demonstration of ^{26}Mg excess
945 in Allende and evidence for ^{26}Al. *Geophys. Res. Lett.* **3**, 109–112.
946 Livermore B. D., Connelly J. N., Moynier F. and Bizzarro M., (2018) Evaluating the
947 robustness of a consensus ^{238}U/^{235}U value for U-Pb geochronology, *Geochim. Cosmochim.*
948 *Acta* **237**, 171–183.
949 Lodders, K. (2003) Solar system abundances and condensation temperatures of the
950 elements. *Astrophys. J.* **591**, 1220–1247.
951 Ludwig K. R. (1980). Calculation of uncertainties of U–Pb isotope data. *Earth Planet.*
952 *Sci. Lett.* **46**, 212–220.
953 Ludwig K. R. (2003) Isoplot/Ex version 3.00, A Geochronological Toolkit for Microsoft
954 Excel. Berkeley Geochronology Center Special Publ. 4, May 30, 2003,
955 http://www.bgc.org/Isoplot3betaManual.pdf).
956 Ludwig K. R. (2009) Squid 2 – A User's manual (rev 2.50). Berkeley Geochronology
957 Center, Special Publication, 100pp.
958 Luu T.-H., Young E. D., Gounelle M. and Chaussidon M. (2015) Short time interval for
959 condensation of high–temperature silicates in the solar accretion disk. *Proc. National Acad.*
960 *Sci.* **112**, 1298–1303.
961 MacPherson G. J., Davis A. M. and Zinner E. K. (1995) The distribution of aluminum
962 - 26 in the early Solar System−A reappraisal. *Meteorit. Planet. Sci.*, **30**, 365–386.
963 MacPherson G. J., Bullock E. S., Janney P. E., Kita N. T., Ushikubo T., Davis A. M.,
964 Wadhwa M. and Krot A. N. (2010) Early solar nebula condensates do not have
965 supracanonical initial ^{26}Al/^{27}Al. *Astrophys. J.* **711**, L117−L121.

MacPherson G. J., Kita N. T., Ushikubo T., Bullock E. S. and Davis A. M. (2012) Well–resolved variations in the formation ages for Ca–Al–rich inclusions in the early solar system. *Earth Planet. Sci. Lett.* **331–332**, 43–54.

MacPherson G. J., Nagashima K., Krot A. N., Doyle P. M. and Ivanova M. A. (2017) ^{53}Mn–^{53}Cr chronology of Ca–Fe silicates in CV3 chondrites, *Geochim. Cosmochim. Acta* **201**, 260–274.

Makide K., Nagashima K., Krot A. N., Huss G. R., Hutcheon I. D., and Bischoff A. (2009) Oxygen- and magnesium-isotope compositions of calcium-aluminum-rich inclusions from CR2 carbonaceous chondrites. *Geochim. Cosmochim. Acta* **73**, 5018-5050.

McKeegan K. D., Chaussidon M. and Robert F. (2000) Incorporation of short-lived 10Be in a calcium-aluminum-rich inclusion from the Allende meteorite. *Science* **289**, 1334–1337.

Mostefaoui S., Kita N. T., Togashi S., Tachibana S., Nagahara H. and Morishita Y. (2002) The relative formation ages of ferromagnesian chondrules inferred from their initial aluminum–26/aluminum–27 ratios. *Meteorit. Planet. Sci.* **37**, 421–438.

Nagashima K., Krot A. N. and Komatsu M. (2017) ^{26}Al–^{26}Mg systematics in chondrules from Kaba and Yamato 980145 CV3 carbonaceous chondrites, *Geochim. Cosmochim. Acta* **201**, 303–319.

Nagashima K., Kita N. T., and Luu T.-H. (2019) ^{26}Al–^{26}Mg systematics of chondrules. In:, *Chondrules: Records* of *Protoplanetary Disk Processes* (eds. S. Russell, H. Connolly Jr. and A. Krot), Cambridge Planetary Science, *Cambridge Univ. Press.* Cambridge. pp. 247–275.

Norris T. L., Gancarz A. J., Rokop D. J. and Thomas K. W. (1983) Half-life of ^{26}Al. *J. Geophys. Res.-Solid Earth* **88**, B331–B333.

989 Pape P., Mezger K., Bouvier A.-S. and Baumgartner L. P. (2019) Time and duration of
990 chondrule formation: Constraints from ^{26}Al–^{26}Mg ages of individual chondrules. *Geochim.*
991 *Cosmochim. Acta* **244**, 2019, 416–436,
992 Park C., Nagashima K., Krot A. N., Huss G. R., Davis A. M., and Bizzarro M. (2017)
993 Calcium-aluminum-rich inclusions with fractionation and unidentified nuclear effects (FUN
994 CAIs): II. Heterogeneities of magnesium isotopes and 26Al in the early Solar System inferred
995 from in situ high-precision magnesium-isotope measurements. *Geochim. Cosmochim. Acta*
996 **201**, 6-24.
997 Richter S., Alonso A., De Bolle W., Kühn H., Verbruggen A., Wellum R. and Taylor P.
998 (2005) Re–certification of a series of uranium isotope reference materials: IRMM–183,
999 IRMM–184, IRMM–185, IRMM–186 and IRMM–187. *International J. Mass Spectrom.*,
1000 **247**, 37–39.
1001 Richter S., Eykens R., Kühn H., Aregbe Y., Verbruggen A., Weyer S. (2010) New
1002 average values for the ^{238}U/^{235}U isotope ratios of natural uranium standards. *International J.*
1003 *Mass Spectrom.*, **295**, 94–97.
1004 Rocholl, A., and Jochum, K. P. (1993) Th, U and other trace elements in carbonaceous
1005 chondrites: Implications for the terrestrial and solar-system Th/U ratios. *Earth Planet. Sci.*
1006 *Lett.* **117**, 265–278.
1007 Sano Y., Takada M., Takahata N., Fujiya W. and Sugiura N. (2014) Ion microprobe Al–
1008 Mg dating of single plagioclase grains in an Efremovka chondrule. *Geochem. J.* **48**, 133–144.
1009 Schrader D. L., Nagashima K., Krot A. N., Ogliore R. C., Yin Q.–Z., Amelin Y., Stirling
1010 C. H., Kaltenbach A. (2017) Distribution of ^{26}Al in the CR chondrite chondrule–forming
1011 region of the protoplanetary disk. *Geochim. Cosmochim. Acta* **201**, 275-302.
1012 Shu F. H., Shang S., Gounelle M., Glassgold A. E. and Lee T. (2001) The origin of
1013 chondrules and refractory inclusions in chondritic meteorites. *Astrophys. J.* **548**, 1029–1050.

1014 Srinivasan G., Huss G. R. and Wasserburg G. J. (2000) A petrographic, chemical, and
1015 isotopic study of calcium–aluminum-rich inclusions and aluminum-rich chondrules from the
1016 Axtell (CV3) chondrite. *Meteorit. Planet. Sci.* **35**, 1333–1354.
1017 Stacey J. S., Kramers J. D. (1975). Approximation of terrestrial lead isotope evolution by
1018 a two–stage model. *Earth Planet. Sci. Lett.* **26**, 207–221.
1019 Stirling C. H., Halliday A. N., Potter E.–K., Andersen M. B. and Zanda, B. (2006) A low
1020 initial abundance of ^{247}Cm in the early Solar System and implications for r–process
1021 nucleosynthesis. *Earth Planet. Sci. Lett.* **251**, 386–397.
1022 Tanaka T., Nakamura N., Masuda A. and Onuma N. (1975) Giant olivine chondrule as a
1023 possible later-stage product in the nebula. *Nature* **256**, 27-28.
1024 Tatsumoto M., Knight R. J. and Allegre C. J., (1973) Time differences in the formation
1025 of meteorites as determined from the ratio of ^{207}Pb to ^{206}Pb. *Science* **180**, 1279–1283.
1026 Tatsumoto M., Unruh D. M. and Desborough, G. A. (1976) U-Th-Pb and Rb-Sr
1027 systematics of Allende and U–Th–Pb systematics of Orgueil. *Geochim. Cosmochim. Acta* **40**,
1028 617–634.
1029 Ushikubo T., Nakashima D., Kimura M., Tenner T. and Kita, N. T. (2013)
1030 Contemporaneous formation of chondrules in distinct oxygen isotope reservoirs. *Geochim.*
1031 *Cosmochim. Acta* **109**, 280–295.
1032 Verbruggen A., Alonso A., Eykens R., Kehoe F., Kühn H., Richter S. and Aregbe, Y.
1033 (2008) Preparation and Certification of IRMM–3636, IRMM–3636a and IRMM–3636b:
1034 OPOCE, 24pp.
1035 Villeneuve J., Chaussidon M. and Libourel G. (2009) Homogeneous distribution of ^{26}Al
1036 in the solar system from the Mg isotopic composition of chondrules. *Science* **325**, 985–988.

1037 Wasserburg G. J., Wimpenny J., and Yin Q.-Z. (2012) Mg Isotopic Heterogeneity, Al-
1038 Mg Isochrons, and Canonical $^{26}Al/^{27}Al$ in the Early Solar System. *Meteorit. Planet. Sci.* **47**,
1039 1980–1997.
1040 Weisberg M. K., McCoy T. J. and Krot A. N. (2006) Systematics and evaluation of
1041 meteorite classification. In *Meteorites and the early solar system II* (eds. D. S. Lauretta and
1042 H. Y. McSween Jr.). The University of Arizona Press, Tucson. pp. 19–52.
1043 Wogelius R. A. and J. V. Walther (1991) Olivine dissolution at 25°C: Effects of pH,
1044 CO2, and organic acids. *Geochim. Cosmochim. Acta* **55**, 943–954.
1045 Yin Q.–Z., Amelin Y., Koefoed P., Huyskens M. H. and Sanborn M. (2016) U–Pb
1046 Dating of the Allende CAI A63 1–C–1, *78th Annual Meeting of the Meteoritical Society*,
1047 27–31 July, Berkeley, US.
1048
1049 **Figure captions:**
1050
1051 Figure 1: Back-scattered electron images of a section of the mega-chondrule and locations of
1052 EDS points. (a) Overview of the texture of a cross section of the mega-chondrule. (b) Details
1053 of a local area of the previous image. The mineral phases present are olivine (Ol),
1054 clinopyroxene (cpx) and mesotasis (meso). EDS points are shown as small ovals. (c) Details
1055 of the texture of the mega-chondrule. Note the micro-crystalline texture of the mesostasis. In
1056 addition to olivine and clinopyroxene, chromium spinel (Cr-sp) is present in this section.
1057
1058 Figure 2: $^{238}U/^{235}U$ ratio of the mega-chondrule (A25-2). Data from previous studies are
1059 shown for comparison. Data from pooled and single chondrules are distinguished. Values of
1060 the $^{238}U/^{235}U$ ratio measured in Allende bulk rock are also shown. Data sources: Amelin et al.

1061 (2010), Brennecka et al. (2010, 2015), Connelly et al. (2012), Goldmann et al. (2015), and
1062 Stirling et al. (2005, 2006).

1063

1064 Figure 3: $^{27}Al/^{24}Mg$ vs. $\delta^{26}Mg$ plot. Error crosses are given at 2σ level. Error envelop of the
1065 regression is plotted at 2σ level. Reference line corresponding to an initial $(^{26}Al/^{27}Al)_0$ of
1066 $5.25x10^{-5}$ (initial value for solar system) is also shown.

1067

1068 Figure 4: $^{207}Pb/^{206}Pb$ vs. $^{204}Pb/^{206}Pb$ plot showing all data of all steps of the leaching sequence
1069 and residues obtained from the nine fractions of the mega-chondrule. (a): All data are
1070 represented as squares for clarity. Uncertainties are smaller than the symbols. Data points
1071 corresponding to the isotopic composition of average Earth's modern Pb (Stacey and Kramer,
1072 1975), Canyon Diablo Troilite (data from Tatsumoto et al., 1973) are also shown. (b):
1073 Enlargement of (a) showing the trend of the first steps of the leaching procedure toward the
1074 isotopic composition of average Earth's modern Pb.

1075

1076 Figure 5: $^{207}Pb/^{206}Pb$ vs. $^{204}Pb/^{206}Pb$ plot of the Allende matrix measurements. Fractions with
1077 $^{206}Pb/^{204}Pb$ ratios higher than 10 (i.e. $^{204}Pb/^{206}Pb < 0.1$ on the plot) are the three powder
1078 fractions while the fractions with $^{206}Pb/^{204}Pb$ ratios lower than 10 are grain fractions. All
1079 dates are calculated using a $^{238}U/^{235}U$ ratio measured in Allende bulk rock ($^{238}U/^{235}U$ =
1080 137.751, Amelin et al., 2010). Also plotted the composition of terrestrial Pb according to
1081 Stacey and Kramer (1975) and primordial Pb assumed to be either the composition of Canyon
1082 Diablo Troilite (CDT, according to Tatsumoto et al., 1973) or Nantan troilite according to
1083 Blichert-Toft et al., 2010).

1084

1085 Figure 6: Assessment of the efficiency of the different acid leaching steps involved in the
1086 three chemical protocols in separating initial, terrestrial and radiogenic Pb components
1087 present in the mega-chondrule A25-2. The percentages of Pb, U and Th removed from
1088 contents as well as the $^{206}Pb/^{204}Pb$ ratios are shown for each steps of the three protocols.

1089

1090 Figure 7: $^{207}Pb^*/^{206}Pb^*$ model ages calculated assuming an initial Pb composition similar to
1091 CDT (Tatsumoto et al., 1973). The plotted data are those remaining after the fifth step of data
1092 filtering (residues and HF steps) and are sorted according to the leaching sequence of the
1093 different protocols.

1094

1095 Figure 8: $^{207}Pb/^{206}Pb$ vs. $^{204}Pb/^{206}Pb$ plot showing Regression 7. (a) Plot showing the
1096 recombined HF (L7 and L8) and HF+residue steps of the leaching protocols applied to
1097 fractions A66 and A68. (b) Plot showing the propagation of the regression error envelop
1098 towards the alleged compositions of initial Pb of the mega-chondrule A25-2. These
1099 compositions are CDT (Tatsumo et al., 1973), Nantan troilite (Blichert-Toft et al., 2010) and
1100 Allende matrix (this work).

1101

1102 Figure 9: Comparison of Pb-Pb age of CV3 (including Allende), L3 and CR chondrules.
1103 Average CV3 CAIs age is also shown (see text for further details). Filled symbols: ages
1104 calculated with a $^{238}U/^{235}U$ ratio measured in the same chondrule. Open symbols: ages
1105 calculated with an assumed $^{238}U/^{235}U$ ratio. Data of Allende chondrules from Amelin and
1106 Krot, 2007; Connelly et al., 2008; Connelly and Bizzarro, 2009; Connelly et al., 2012

(Allende chondrules) and Bollard et al., 2017 (L3 and CR chondrules). The published ages of Allende chondrules using an assumed $^{238}U/^{235}U$ ratio, were recalculated using a $^{238}U/^{235}U$ ratio of 137.786±0.004 (average value of Allende chondrules according to Brennecka et al., 2015). The published CR and L3 chondrule ages using an assumed $^{238}U/^{235}U$ ratio, were recalculated using a $^{238}U/^{235}U$ ratio of 137.794±0.027 (best estimate for the solar system according to Goldmann et al., 2015). Data of Allende CAIs are from Jacobsen et al., 2008; Amelin et al., 2010 and Yin et al., 2015. Data of CV3 CAIs are from Amelin et al., 2002; Bouvier et al., 2011; Connelly et al., 2012. All the published ages calculated with a $^{238}U/^{235}U$ ratio measured in the same chondrule or CAI were not recalculated.

Table 1: Representative electron microprobe analyses of the main mineral phases present in the mega-chondrule.

Table 2: Al-Mg systematics in mega-chondrule A25-2 mineral phases analysed by MC-ICP-MS.

Table 3: U-Pb systematics from Allende matrix.

Table 4: U-Pb-Th concentrations and $^{204}Pb/^{206}Pb$ and $^{207}Pb/^{206}Pb$ isotopic ratios measured by SHRIMP II in mineral phases and mesostasis from Allende mega-chondrule. The values of the standards are also given.

Table 5: Summary of the step-by-step process of data filtering and regression construction.

Table1

Table 1: Represntative compositions of minerals (wt%).

mineral	ol	Ca px	Cr-spinel	mesostasis
SiO_2	37.8	49.7	0.14	49.0
TiO_2	b.d.	0.41	0.62	0.59
Al_2O_3	0.05	6.9	23.7	21.0
Cr_2O_3	0.13	1.50	42.9	0.10
FeO	25.2	13.8	24.4	7.0
MnO	0.20	0.24	0.21	0.13
MgO	36.2	19.6	7.3	5.3
CaO	0.20	7.6	b.d.	12.3
Na_2O	b.d.	b.d.	b.d.	2.8
K_2O	b.d.	b.d.	b.d.	0.05
total	99.8	99.7	99.3	98.2
Composition[†]	71.9	59.8, 16.6		

[†]forsterite, and enstatite and wollastonite contents are shown for olivine and Ca pyroxene, respectively.

b.d.: below detection limit

Table2

Table 2: Results of Al-Mg isosope analyses using MC-SIMS.

analysis #	phase	$^{27}Al/^{24}Mg$	$\delta^{26}Mg$ (‰)
px#1	high-Ca px	0.415 ± 0.014	0.006 ± 0.101
px#2	high-Ca px	0.261 ± 0.009	0.058 ± 0.085
px#3	high-Ca px	0.244 ± 0.008	-0.003 ± 0.081
px#4	high-Ca px	0.213 ± 0.007	-0.035 ± 0.094
ol#1	olivine	0.00143 ± 0.00005	-0.051 ± 0.083
ol#2	olivine	0.00128 ± 0.00004	-0.048 ± 0.083
ol#3	olivine	0.00126 ± 0.00004	-0.054 ± 0.081
sp#1	Cr-spinel	2.2 ± 0.2	0.051 ± 0.181
sp#2	Cr-spinel	3.3 ± 0.3	0.075 ± 0.177

Table3

Table 3: U-Pb isotopic data of the Allende matrix fractions

							Sample (Radiogenic + Initial Pb) Isotope Ratios						
Sample	Wt. mg	Pb ppm	mol % $^{206}Pb^{*}$	Pb* / Pbc	Pbc ppm	$^{206}Pb/^{204}Pb$	$^{206}Pb/^{204}Pb$	% err ±	$^{204}Pb/^{206}Pb$	% err ±	$^{207}Pb/^{206}Pb$	% err ±	corr. coef. 7/6-4/6
(a)	(b)	(c)	(d)	(d)	(d)	(e)	(g)	(f)	(g)	(f)	(g)	(f)	
Allende matrix													
A116-1 (powder)	1.41	21.55	0.50	0.46	14.73	18.649	18.649	0.025	0.054	0.025	0.831	0.029	-0.002
A116-2 (powder)	1.19	1.39	0.33	0.24	1.12	13.982	13.980	0.021	0.072	0.021	0.928	0.021	0.177
A116-3 (powder)	1.49	1.06	0.20	0.12	0.95	11.596	11.593	0.034	0.086	0.034	1.005	0.025	0.302
A116-4 (fragments)	1.58	1.36	0.04	0.02	1.34	9.661	9.658	0.039	0.104	0.039	1.088	0.032	0.234
A116-5 (fragments)	0.91	1.50	0.03	0.02	1.47	9.621	9.617	0.045	0.104	0.045	1.092	0.024	0.677
A116-6 (fragments)	0.81	1.34	0.03	0.02	1.32	9.610	9.604	0.063	0.104	0.063	1.092	0.028	0.665
A117-1 (fragments)	0.50	1.23	0.03	0.01	1.22	9.589	9.578	0.092	0.104	0.092	1.094	0.052	0.777
A117-2 (fragments)	0.51	1.19	0.05	0.02	1.16	9.796	9.785	0.099	0.102	0.099	1.084	0.047	0.758
A117-3 (fragments)	0.42	1.16	0.05	0.03	1.13	9.849	9.836	0.113	0.102	0.113	1.082	0.060	0.807
A117-4 (fragments)	0.15	0.93	0.03	0.01	0.92	9.596	9.550	0.392	0.105	0.392	1.095	0.192	0.966

(a) labels for fractions.
(b) Nominal fraction weights.
(c) Nominal U and total Pb concentrations subject to uncertainty of weight.
(d) Pb* and Pbc represent radiogenic and common Pb, respectively; mol % $^{206}Pb^{*}$ with respect to radiogenic, blank and initial common Pb.
(e) Measured ratio corrected for spike and fractionation only.
(f) Errors are 2-sigma, propagated using the algorithms of Schmitz and Schoene (2007) and Crowley et al. (2007).
(g) Corrected for fractionation, spike, and blank Pb.

Table4

Table 4: U-Th-Pb contents and Pb isotopic ratios measured in-situ by SHRIMP II in mega-chondrule A25-2 in the different mineral phases and mesostasis from Allende mega-chondrule

Sample name	$^{204}Pb/^{206}Pb$	1σ err. (%)	$^{207}Pb/^{206}Pb$	1σ err. (%)	$^{208}Pb/^{206}Pb$	1σ err. (%)	Concentrations			
							^{204}Pb (ppm)	Yb (ppm)	U (ppm)	Th (ppm)
Standards										
NIST612-1.4	0.0606	6.0	0.9187	2.9	2.2042	2.7	-	-	-	-
NIST612-1.5	0.0594	6.1	0.9239	2.9	2.1851	2.8	-	-	-	-
NIST612-1.6	0.0595	6.6	0.9022	3.1	2.1666	3.0	-	-	-	-
NIST612-1.7	0.0565	6.6	0.8962	3.1	2.1451	2.9	-	-	-	-
NIST612-1.8	0.0594	6.4	0.9260	3.0	2.1508	2.9	-	-	-	-
NIST612-1.10	0.0597	6.1	0.9114	2.9	2.1558	2.8	-	-	-	-
NIST612-1.11	0.0615	6.1	0.9099	2.9	2.1590	2.8	-	-	-	-
NIST612-12	0.0600	6.2	0.9008	2.9	2.1378	2.8	-	-	-	-
NIST612-13	0.0595	6.2	0.9182	2.9	2.1895	2.8	-	-	-	-
NIST612-14	0.0603	6.3	0.9164	3.0	2.1753	2.9	-	-	-	-
NIST612-15	0.0611	6.2	0.9103	3.0	2.1464	2.8	-	-	-	-
BCR1.1	0.0543	7.7	0.8581	3.5	2.0862	3.4				
BCR1.2	0.0532	7.4	0.8344	3.4	2.0625	3.2				
BCR1.3	0.0529	7.1	0.8180	3.3	2.0193	3.1	0.6600	3.5000	1.6900	6.2000
BCR1.4	0.0554	7.5	0.8289	3.5	2.0805	3.3				
BCR1.5	0.0558	6.7	0.8240	3.2	2.0608	3.0				
BCR1.6	0.0533	6.7	0.8218	3.1	2.0324	3.1				
BIR-1.1	0.0584	57.5	0.8945	27.1	2.2993	25.4	0.0107	0.1098	0.0013	0.0030
BIR-2	0.0601	37.8	0.9116	17.9	1.9439	17.6	0.0230	0.1098	0.0038	0.0030
Analysed phases in Allende mega-chondrule A25-2										
olivine										
All_Oliv-10.1	0.4663	150.4	0.6446	172.6	2.6463	140.7	0.0031	0.0439	0.0000	0.0000
All_oliv-1.1	3.6074	156.9	6.8268	156.2	19.7013	140.9	0.0015	0.0659	0.0013	0.0045
All_oliv4.1	0.1412	77.1	1.0162	52.4	3.0516	48.0	0.0061	0.0659	0.0000	0.0000
All_oliv7.1	0.1634	139.3	0.6229	112.6	1.1444	115.7	0.0031	0.0439	0.0000	0.0000
Mesostasis										
All_Meso-10.1	0.0182	143.7	0.6428	43.0	1.2928	42.9	0.0015	0.4613	0.0189	0.1071
All_mesos6.1	0.0394	82.3	0.7701	33.7	1.4608	34.3	0.0031	1.0983	0.0403	0.1754
All_mesos7.1	0.0397	57.4	0.7499	23.8	1.6937	23.0	0.0061	2.3724	0.0643	0.3241
All-meso-9	0.0262	56.0	0.6682	19.8	1.1354	20.8	0.0107	1.8232	0.1223	0.5249
Pyroxene										
All-py-1	0.0142	227.9	0.7769	57.4	1.6472	57.9	0.0000	1.4059	0.0050	0.0342
All-py-2	0.1057	168.8	0.9112	102.5	1.4254	109.7	0.0000	1.2521	0.0000	0.0030
All-py-3	bdl	-	0.4481	78.1	1.1692	71.8	0.0000	2.5701	0.0050	0.0327
All-py-5	bdl	-	0.9552	105.8	2.1163	103.1	0.0000	0.7249	0.0000	0.0030
Cr-spinel										
All-CrSp-3	0.1144	158.5	1.0735	97.4	1.5713	105.7	0.0015	0.0000	0.0000	0.0000
All-CrSp-4	0.0207	335.9	1.2064	92.6	2.2311	94.0	0.0000	0.1318	0.0050	0.0164
All-CrSp-2	bdl	-	0.9233	136.6	3.1830	122.5	0.0000	0.1318	0.0000	0.0000

bdl: below detection limit

Table5

Table 5. Summary of isochron regressions and model dates

Regression	# points	Isochron age	+/-	MSWD	PoF	Minimum age	weighted average $^{207}Pb/^{206}Pb$ model ages	+/-	MSWD	PoF	Data included in regression
1	69	4593	23	584	0	4570	4545.9	8.0	649	0	all mega-chondrule data
2	41	4574	21	341	0	4553	4559.3	6.7	307	0	The earliest washes (water, acetone, dilute acids up to 0.5M HNO3) are removed
3	33	4577	23	382	0	4554	4560.5	7.5	345	0	Fractions containing <4 pg 206Pb are removed
4	30	4568.7	5.2	18	0	4563.5	4564.1	1.8	19	0	Fractions with extreme U-Pb discordance (>500%) are removed
5	19	4567.5	4.1	7.2	0	4563.4	4566.7	1.3	6.8	0	HF leachates and residues
6	8	4564.5	7.7	5.7	0	4556.8	4565.8	1.9	5.0	0	A66+A68 HF leachates and residues - recombined, and A31 residues
7	5	4568.5	3.0	1.6	0.20	4565.5	4566.7	0.8	1.6	0.18	A66+A68 HF leachates and residues - recombined
8	6	4566.7	0.8	1.6	0.18	4565.9					A66+A68 HF leach. and resid. - recombined + primordial Pb (Tatsumoto)
9	6	4564.7	2.0	2.9	0.022	4562.7					A66+A68 HF leach. and resid. - recombined + primordial Pb (Blichert-Toft)
10	11	4564.9	1.4	2.2	0.018	4563.5					A66+A68 HF leach. and resid. - recombined + Allende matrix fragments (n=6)
11	9	4565.0	0.8	2.2	0.018	4564.2					A66+A68 HF leach. and resid. - recombined + Allende matrix fragments (n=4) with most primitive Pb isotopic composition.
101	3	4371	150	122	0	4221					Allende matrix - powders
101	7	4597	180	22	0	4417					Allende matrix - fragments - all
102	6	4606	30	0.30	0.79	4576					Allende matrix - fragments - A116 5, 6, A117 1-4.

Figure 1

Figure 1

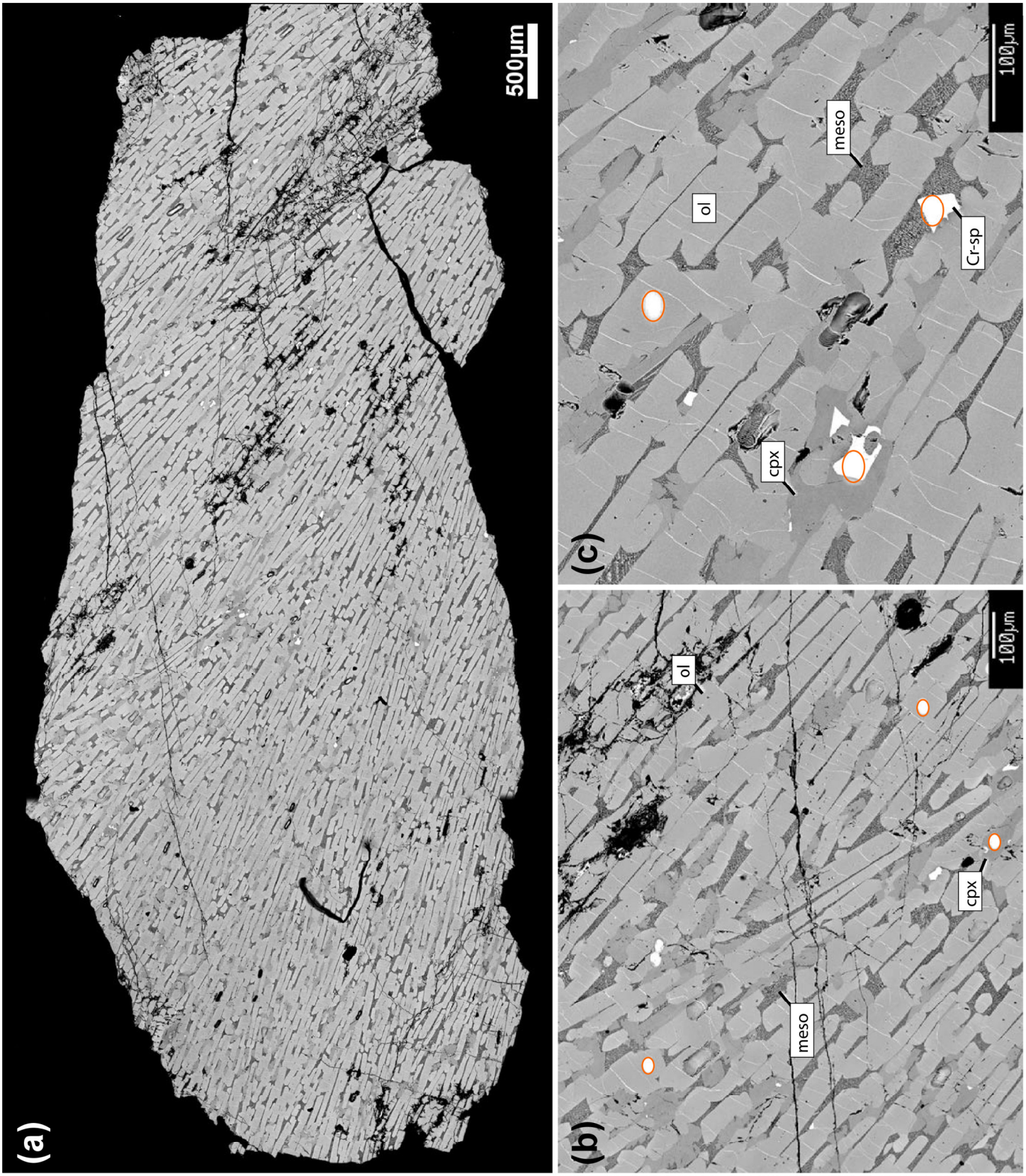

Figure 2

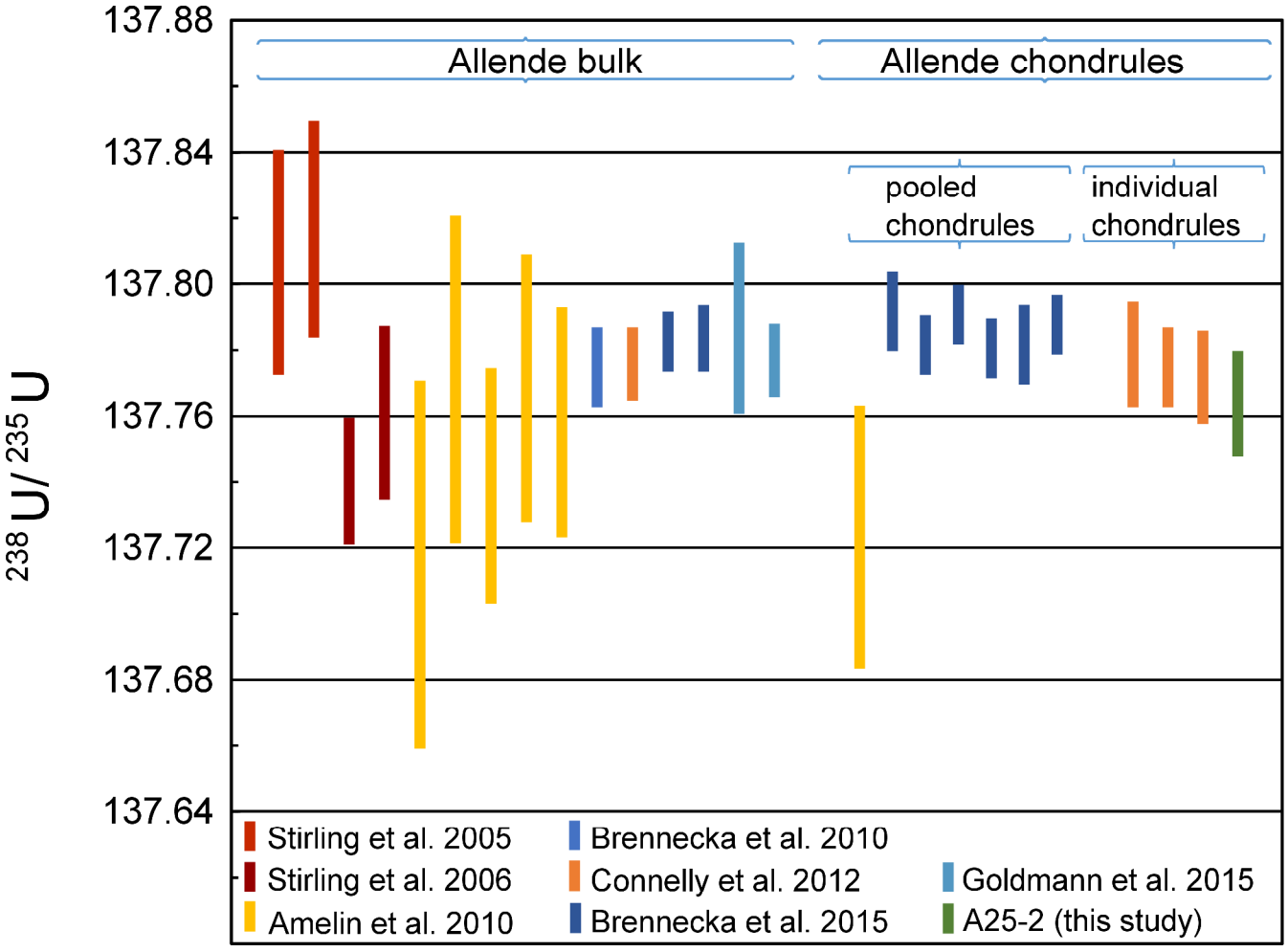

Figure 2

Figure 3

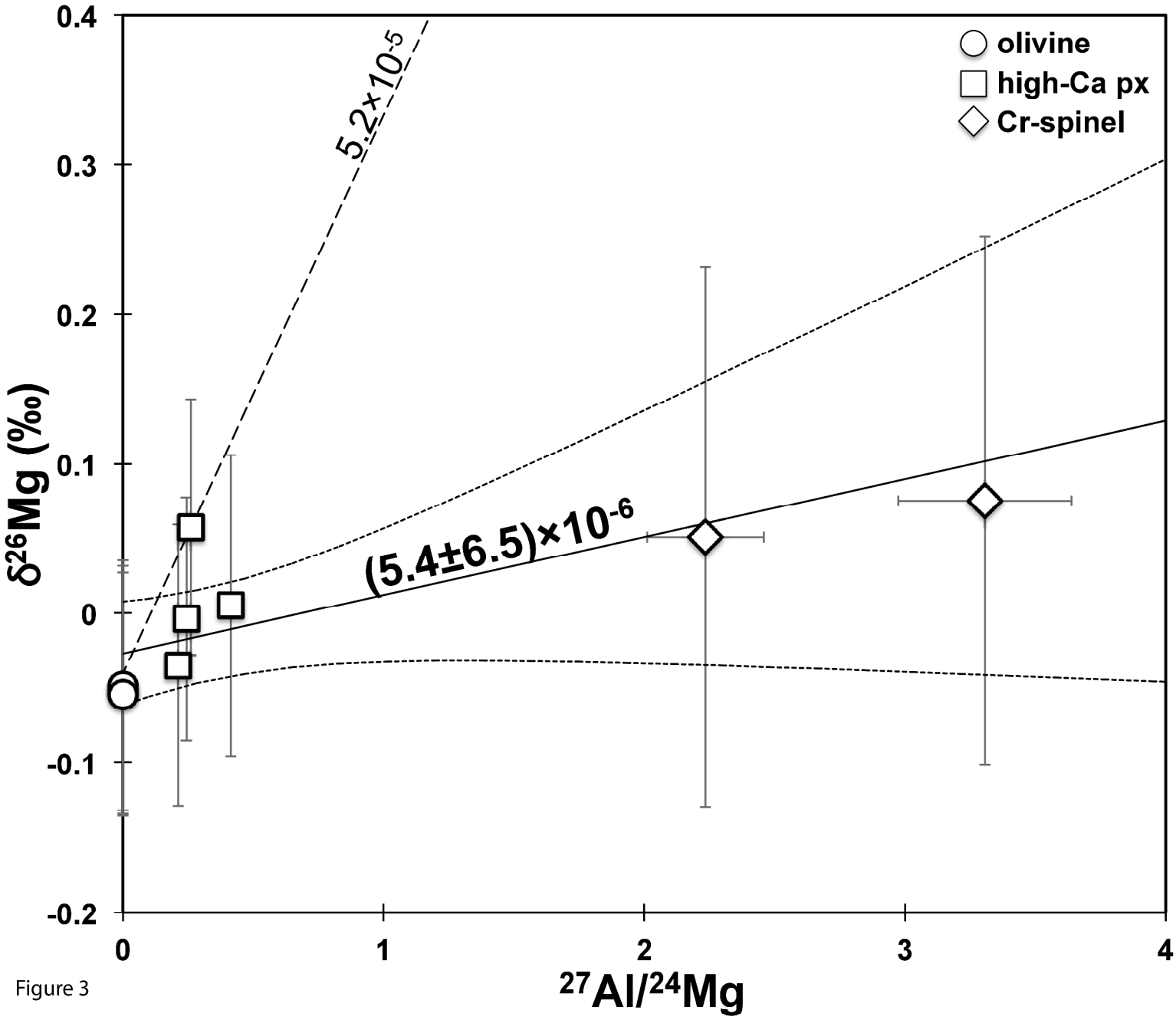

Figure 3

Figure 4

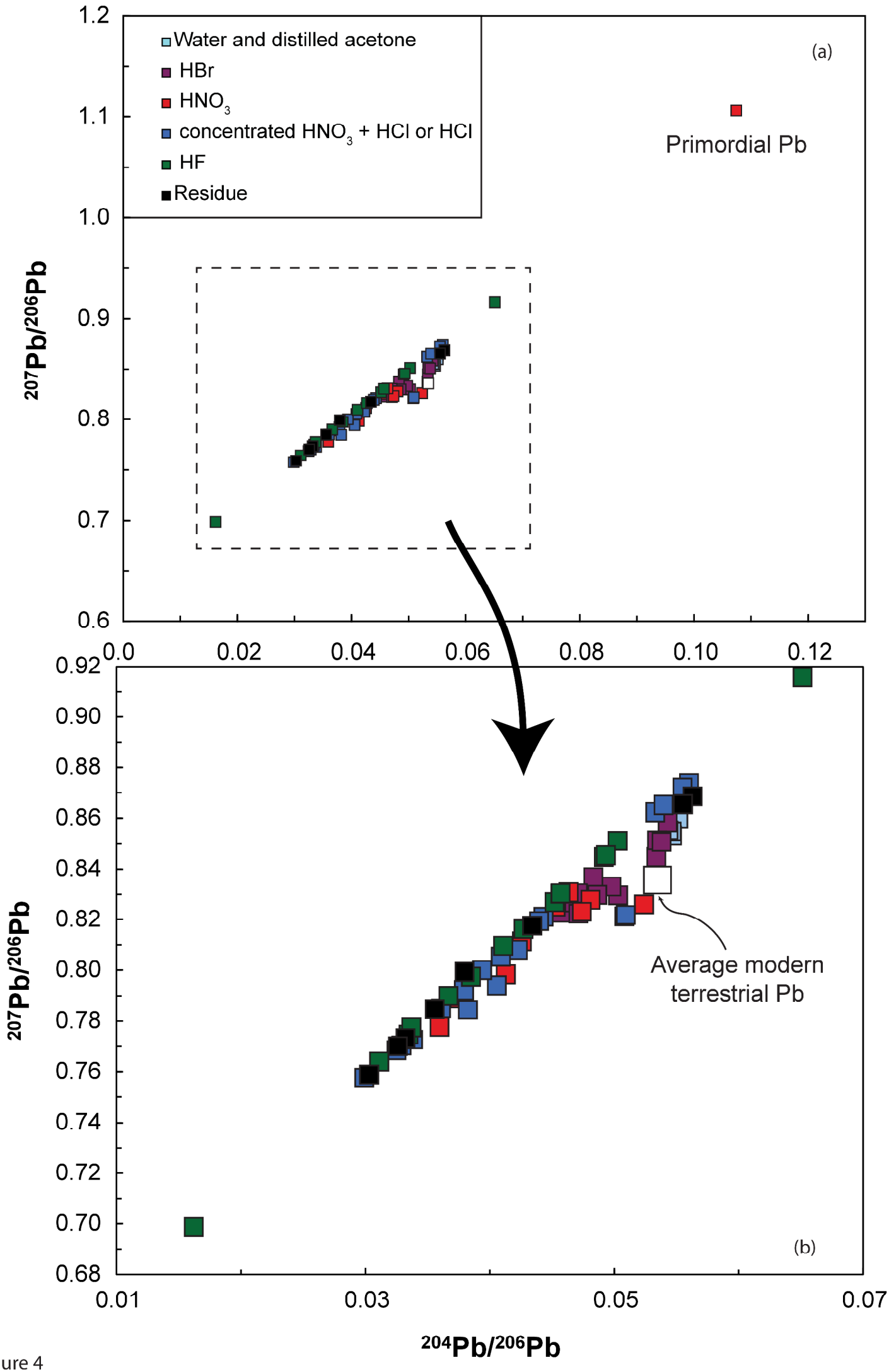

Figure 4

Figure 5

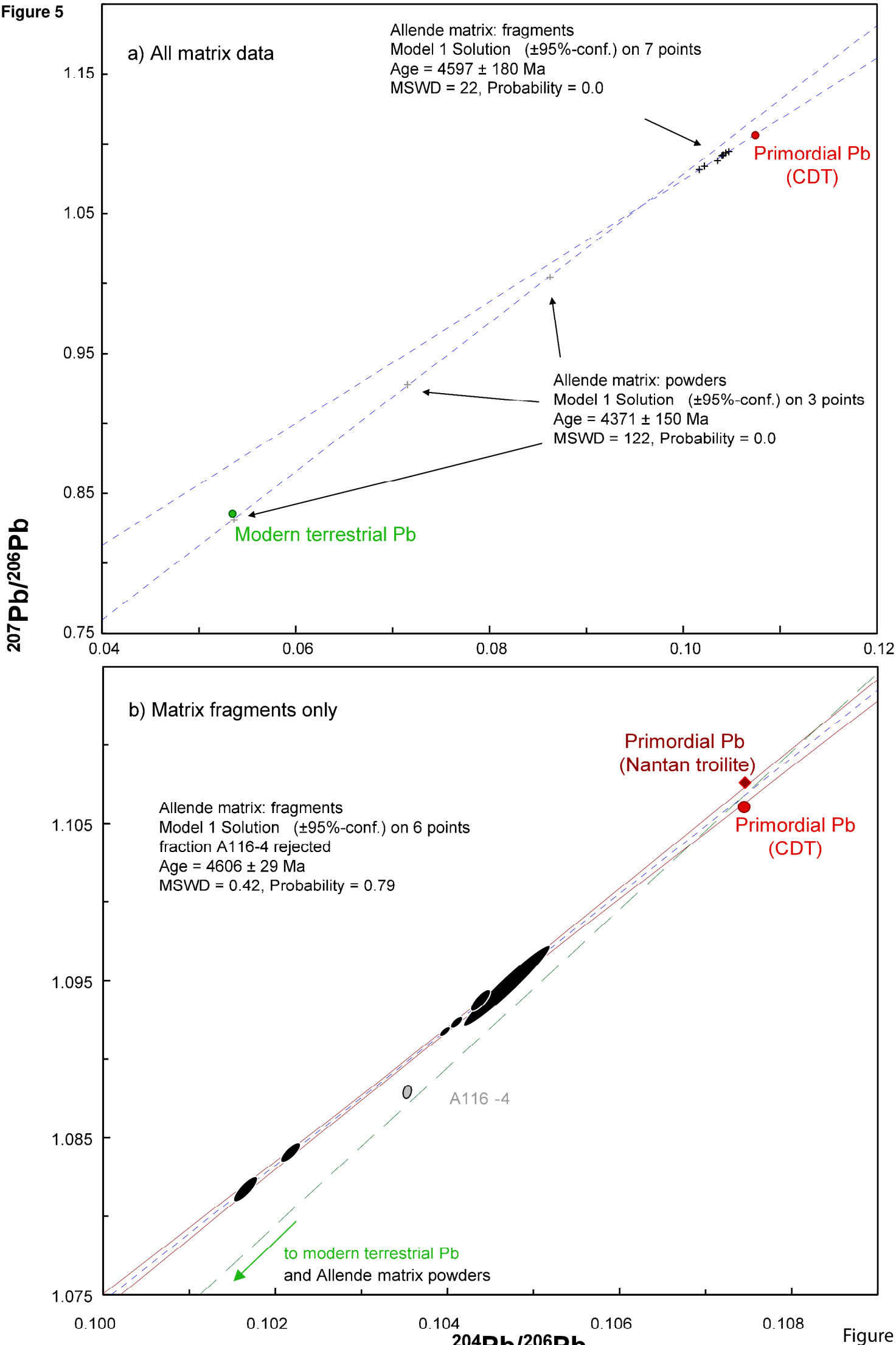

Figure 5

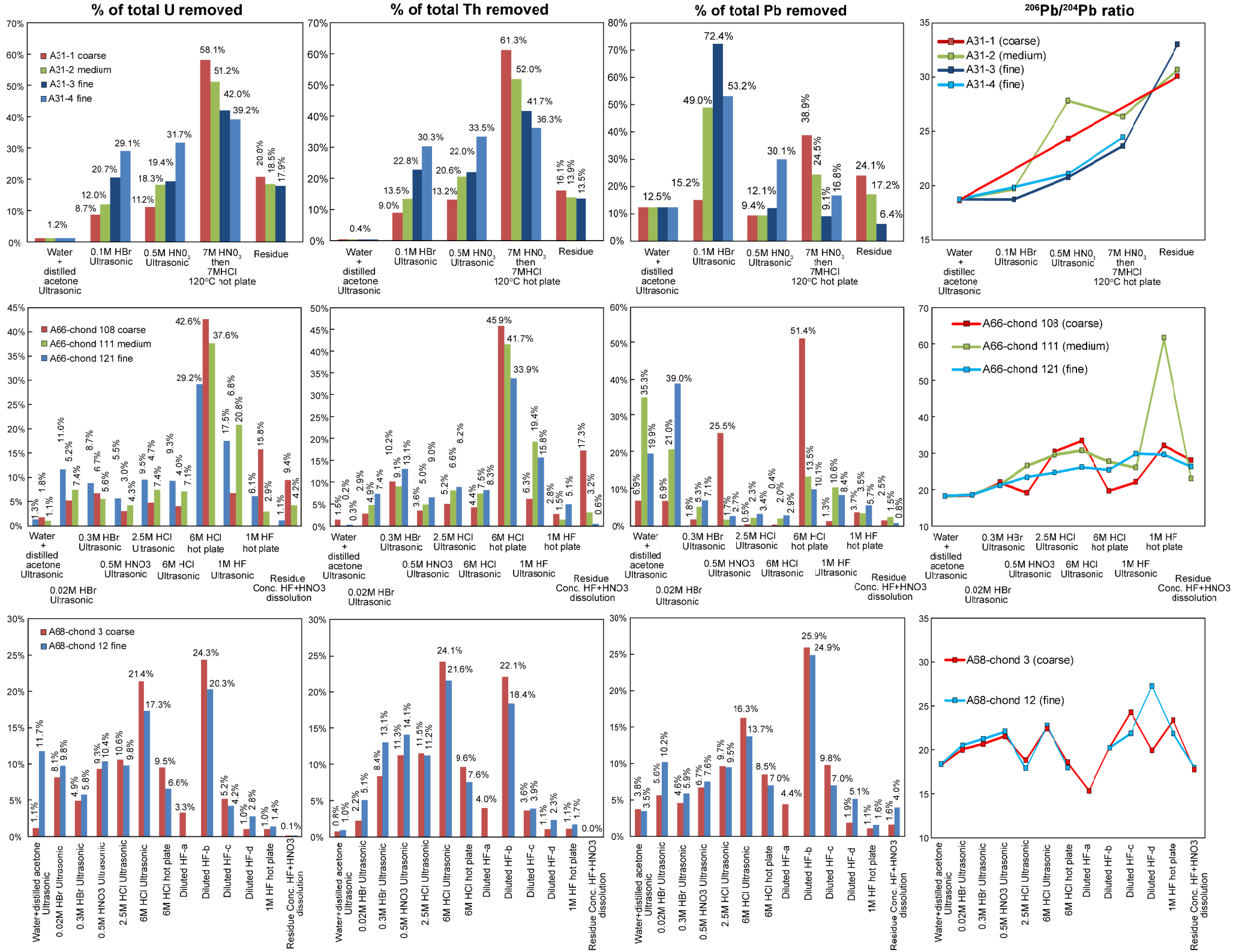
% of total U removed
% of total Th removed
% of total Pb removed
206Pb/204Pb ratio
A31-1 coarse
A31-2 medium
A31-3 fine
A31-4 fine
A31-1 (coarse)
A31-2 (medium)
A31-3 (fine)
A31-4 (fine)
Water + distilled acetone Ultrasonic
0.1M HBr Ultrasonic
0.5M HNO3 Ultrasonic
7M HNO3 then 7MHCl 120°C hot plate
Residue
A66-chond 108 coarse
A66-chond 111 medium
A66-chond 121 fine
A66-chond 108 (coarse)
A66-chond 111 (medium)
A66-chond 121 (fine)
0.02M HBr Ultrasonic
0.3M HBr Ultrasonic
2.5M HCl Ultrasonic
6M HCl hot plate
1M HF hot plate
0.5M HNO3 Ultrasonic
6M HCl Ultrasonic
1M HF Ultrasonic
Residue Conc. HF+HNO3 dissolution
A68-chond 3 coarse
A68-chond 12 fine
A68-chond 3 (coarse)
A68-chond 12 (fine)
Water+distilled acetone Ultrasonic
0.02M HBr Ultrasonic
0.3M HBr Ultrasonic
0.5M HNO3 Ultrasonic
2.5M HCl Ultrasonic
6M HCl Ultrasonic
6M HCl hot plate
Diluted HF-a
Diluted HF-b
Diluted HF-c
Diluted HF-d
1M HF hot plate
Residue Conc. HF+HNO3 dissolution

Figure 6

Figure 7

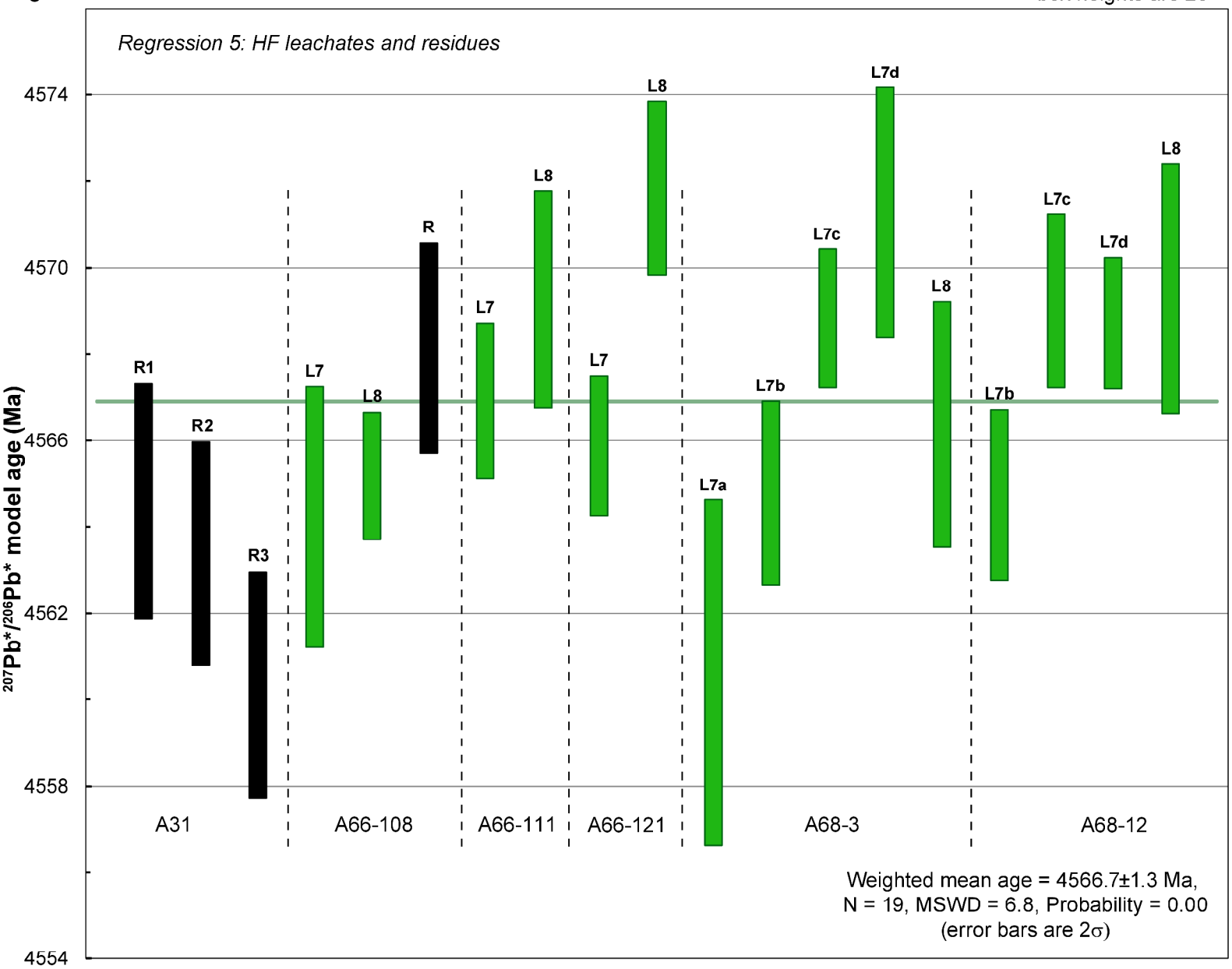

figure 7

Figure 8

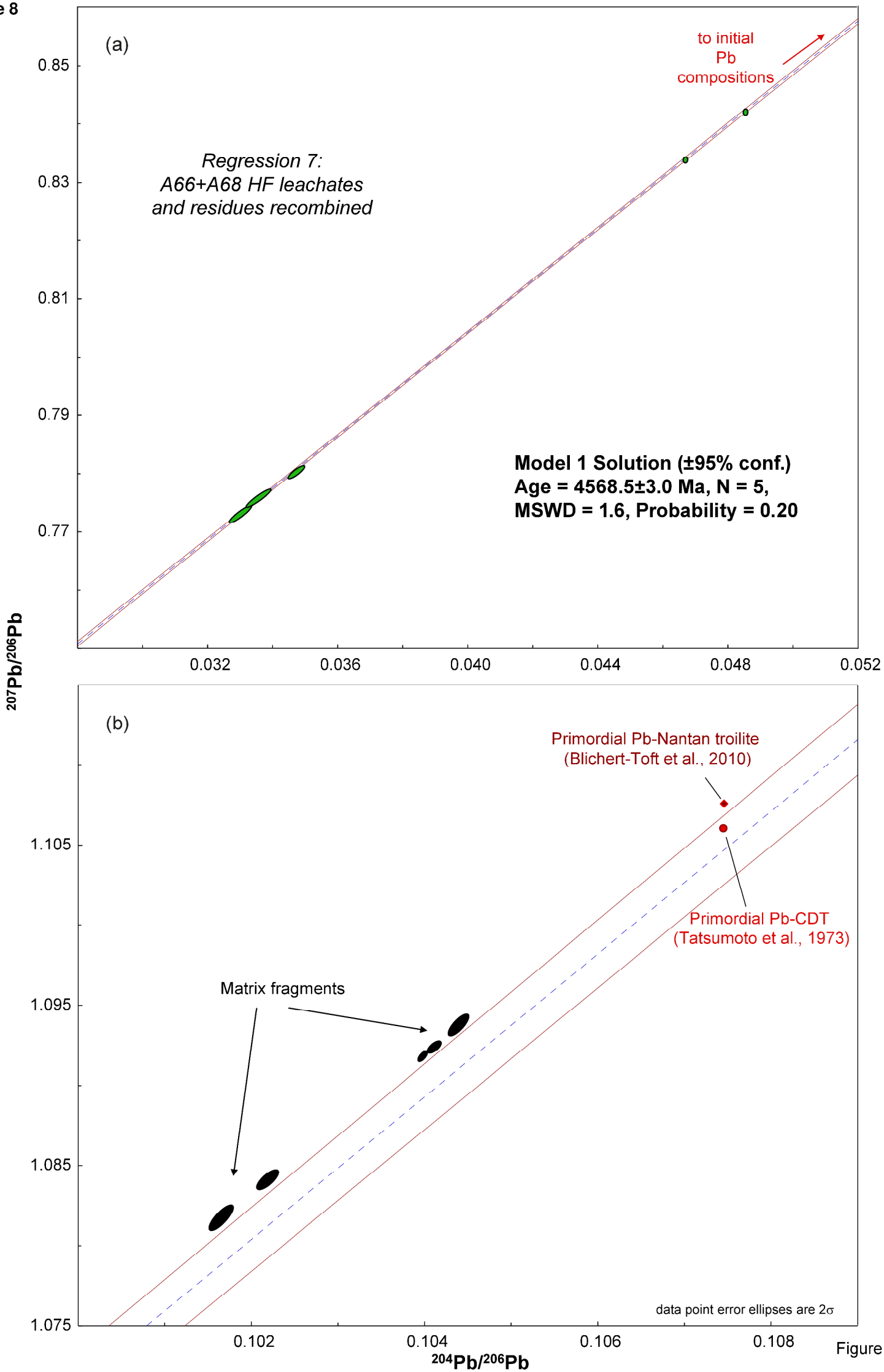

Figure 8

Figure 9

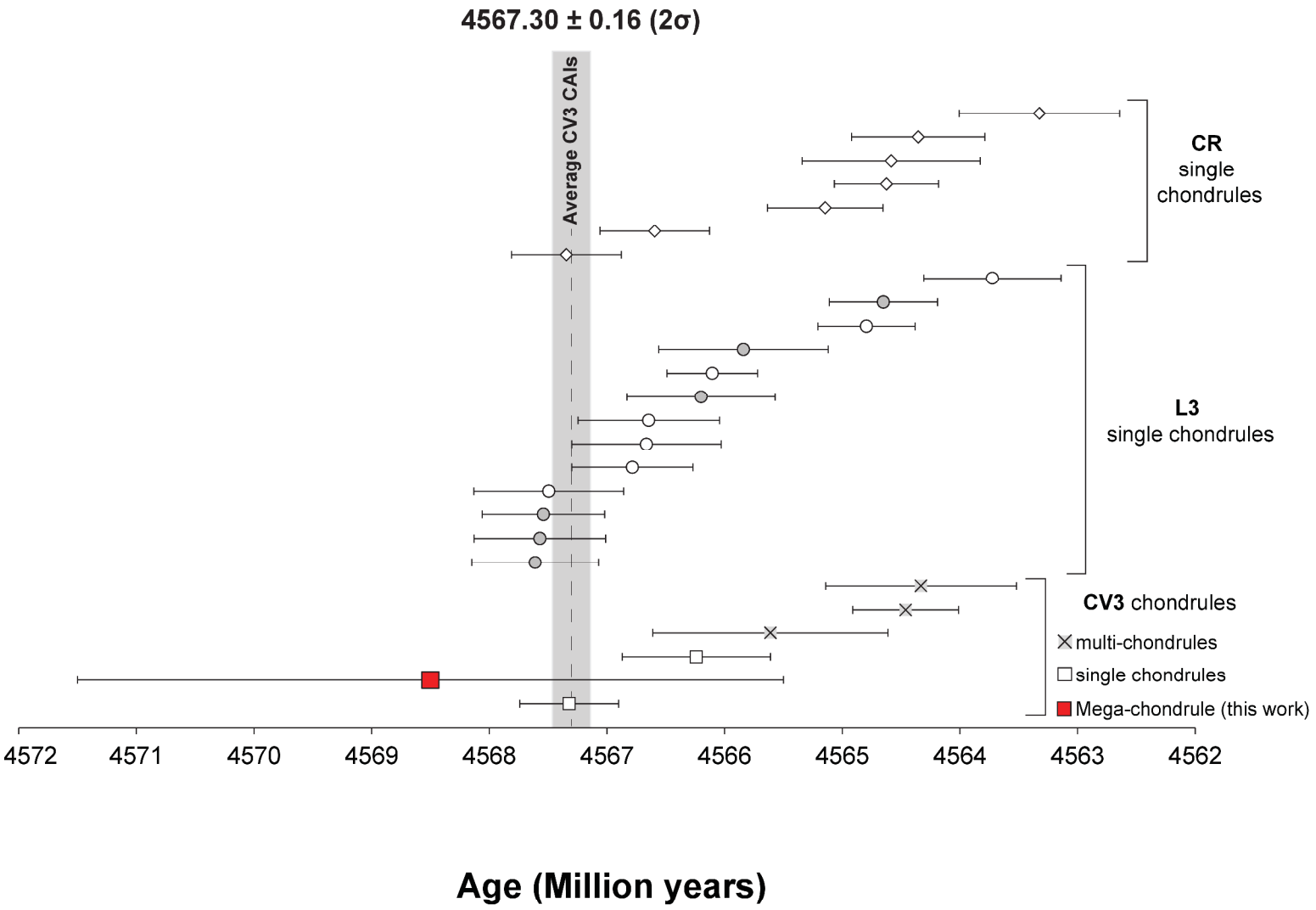

Figure 9